J. Fluid Mech. (2012), *vol.* 701, *pp.* 171–200. © Cambridge University Press 2012
doi:10.1017/jfm.2012.145

Compound viscous thread with electrostatic and electrokinetic effects

D. T. Conroy[1]†, O. K. Matar[1], R. V. Craster[2] and D. T. Papageorgiou[2]

[1] Department of Chemical Engineering, Imperial College London, South Kensington Campus, London SW7 2AZ, UK

[2] Department of Mathematics, Imperial College London, South Kensington Campus, London SW7 2AZ, UK

(Received 5 September 2011; revised 24 January 2012; accepted 12 March 2012; first published online 30 April 2012)

Breakup of an electrified viscous compound jet, surrounded by a dielectric gas, is investigated theoretically. The fluids are considered to be electrolytes and the core fluid viscosity is assumed to be much larger than that of the annular fluid. Axisymmetric configurations are considered with the three fluids bound by a cylindrical electrode that is held at a constant voltage potential. The model equations are investigated asymptotically in the long-wave limit, yielding two cases corresponding to a negligible surface charge with electrokinetic effects and a leaky dielectric model. A linear stability analysis for both cases is performed and the electrical effects are found to have a stabilizing effect, which is consistent with previous investigations of single electrified jet breakup at small wavenumbers. The one-dimensional equations are also solved numerically. The electric field is found to cause satellite formation in the core fluid, which does not occur in the purely hydrodynamic case, with the satellite size increasing with the strength of the electric field.

Key words: capillary flows, electrohydrodynamic effects, nonlinear instability

1. Introduction

Compound electrified jets or threads, consisting of two immiscible, viscous, electrolyte fluids in a core annular arrangement, are important for a class of problems related to micro-encapsulation, ink-jet printing, fibre spinning and drug delivery (Denn 1980; Hertz & Hermanrud 1983; Hardas *et al.* 2000; Lee *et al.* 2001; Loscertales *et al.* 2002). A compound jet is formed by injecting two fluids into ambient air, and as a result of surface tension a capillary instability causes the thread/jet to breakup into droplets. In the case of encapsulation, it is important to be able to control the formation of compound droplets, such as inner droplet size and annular layer thickness, and electric fields are a potentially useful way of achieving this purpose.

Recently, electrified compound jets, formed by ejecting two fluids from a nozzle into an axially applied electric field, have been investigated experimentally to understand the effect of electrospraying on encapsulation (Loscertales *et al.* 2002; Chen *et al.* 2005). This system was also studied theoretically by Higuera (2007), using a leaky dielectric model with a dielectric core and a conducting annular fluid that was solved

† Email address for correspondence: devin.conroy@imperial.ac.uk

https://doi.org/10.1017/jfm.2012.145 Published online by Cambridge University Press

numerically using a boundary element method. In the case of radially applied electric fields, obtained by surrounding the jet with a cylindrical electrode, linear stability analysis has been studied in the case of irrotational (Li, Yin & Yin 2005, 2006) and viscous flow (Li, Yin & Yin 2008) using the leaky dielectric model (Saville 1997). In these investigations the electric field was shown to have a stabilizing effect at small wavenumbers and a destabilizing effect at large numbers. This result is in accordance with findings on single jets (Huebner & Chu 1971) and indicates the possibility of using electric fields to control droplet sizes for encapsulation process.

In the absence of electric field effects, one of the first experimental studies was by Hertz & Hermanrud (1983) who studied compound drop formulation for use in ink-jet printing. The linear stability problem based on one-dimensional models was investigated by Radev & Shkadov (1985) and Sanz & Meseguer (1985) for inviscid flows and Radev & Tchavdarov (1988) for the inclusion of viscosity. The addition of spatial effects on linear theory was studied by Chauhan *et al.* (1996) in the inviscid case and Chauhan *et al.* (2000) for the viscous case; like the single-jet counterpart, compound jets were found to be unstable due to capillary forces. Linear stability analyses of the full problem showed that there are two growing modes: a stretching mode, in which the two fluids move in phase driven by capillary forces at the inner interface and a squeezing mode, in which the interfaces move out of phase driven by capillary forces at the outer interface. Nonlinear studies with large viscosity ratios and in the long-wave limit were investigated by Craster, Matar & Papageorgiou (2005) and with surfactant effects by Craster, Matar & Papageorgiou (2003). A numerical study of the full axisymmetric problem, of a surfactant-free compound jet, was performed by Suryo, Doshi & Basaran (2006).

In this paper we investigate linear and nonlinear compound jet breakup, using long-wave theory, to investigate the breakup process that has so far not been considered in the literature. The long-wave analysis has been used previously by many authors (Papageorgiou 1995; Craster *et al.* 2003, 2005; Conroy *et al.* 2011*a*,*b*), showing good agreement with the full numerical solution for small wavenumbers (Wilkes, Phillips & Basaran 1999; Collins, Harris & Basaran 2007) and has been shown to reduce to the exact solution near breakup for single non-electrified jets. We consider two electrolyte fluids in the coaxial arrangement and surrounded by an electrode that generates a radial electric field. In electrolyte fluids, ions move by diffusion and ion migration in an electric field to form a diffuse layer with a volumetric charge density in the interior of the fluid. A Maxwell stress is present in this case, yielding electrokinetic effects for sufficiently small electric field strengths of a few volts per centimetre. For perfectly conducting, dielectric and leaky dielectric fluids the diffuse layer is very thin or absent and electric stresses occur at fluid–fluid interfaces. In the case of perfect conductors and dielectrics the electric stress acts perpendicular to the interface, whereas in leaky-dielectric fluids free charge accumulates at the interface and a tangential electric stress also develops (Saville 1997). Further, we assume that the core is highly viscous relative to the second annular fluid. From these equations we investigate two cases corresponding to an electrokinetic case, without surface charge, which we show to reduce to the model of Conroy *et al.* (2010) in the limit of very viscous core and thin annular fluid and the leaky-dielectric model.

This paper builds on the work of Craster *et al.* (2005) by including electrostatic and electrokinetic effects, using similar techniques to those developed by the present authors for electrified films (Conroy *et al.* 2010) and single jets (Conroy *et al.* 2011*a*,*b*). The leaky-dielectric model employed in this paper is similar to that of Li *et al.* (2008) but here we solve the nonlinear equations to explore the breakup

https://doi.org/10.1017/jfm.2012.145 Published online by Cambridge University Press

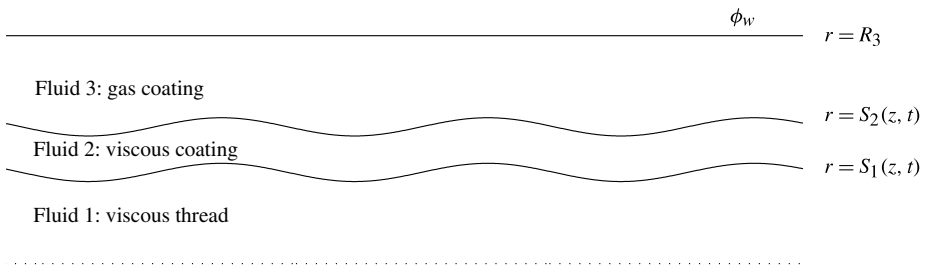


FIGURE 1. Schematic of the flow showing a thin liquid thread coated by another viscous fluid and surrounded by an inviscid gas bounded by an electrode of radius R_3 with a potential ϕ_w; the interfaces are located at $r = S_1(z, t)$ and $r = S_2(z, t)$.

dynamics. Through a parametric study we find that the electric field retards the evolution of the interface and allows for the formation of a satellite. In addition, the electric field can be used to inhibit breakup and allow for the formation of long compound threads. This study demonstrates the potential utility of electric effects in controlling the breakup process which motivates the pursuit of experimental work to verify the predictions and mechanisms found in this paper.

The rest of this paper is organized as follows. In § 2 the general model for electrified compound jets with electrokinetic effects is developed and then reduced in the long-wave limit for a number of cases. In § 3.1 the linear problem is investigated and in § 3.2 the nonlinear problem, that is solved numerically, is presented. Finally, concluding remarks are provided in § 4.

2. Formulation

We consider a compound jet as shown in figure 1, that is bounded by a cylindrical electrode of radius R_3. There are two interfaces located at $r = S_1(z, t)$ and $r = S_2(z, t)$ with initial radii R_1 and R_2 and constant surface tensions γ_1 and γ_2. The third fluid is a dielectric that is bounded by an electrode with a constant potential ϕ_w. The three fluids in the system have densities ρ_i, viscosities μ_i and dielectric permittivities ε_i. Here we take $\mu_3 \ll \mu_{1,2}$; fluid 1 is the core fluid, 2 the annular fluid and 3 is the gas. Both inner fluids are assumed to be symmetric $z : z$ electrolytes and we use the superscript $+, -$ for the cationic and ionic species $n_i^{(+)}, n_i^{(-)}$, respectively where $n_i^{(\pm)}$ are in units of molarity. In addition, there is a charge-neutral species, n_i, from which the ionic species disassociate. (We have chosen to investigate symmetric electrolytes because they are common in systems with a dilute concentration of many types of salt and in systems where ions are formed by water dissociation. In addition, the formulation presented below will apply to asymmetric electrolytes with a straightforward modification to the charges and we refer the reader to a paper by Saville (1997).) Further, a surface species, $\Gamma_i^{(\pm)}$, can be transported to the interface resulting in a surface charge q_i.

2.1. *Governing equations*

The governing equations describing electrified jets have been presented in Saville (1997) so we only present the dimensionless set here. We scale the radial length on the initial radius of the core fluid R_1, the axial length on some scale L, the radial velocity on γ_1/μ_1, the axial velocity on $\delta^{-1}\gamma_1/\mu_1$ ($\delta = R_1/L$), time on $R_1\mu_1/\gamma_1$ and pressure

https://doi.org/10.1017/jfm.2012.145 Published online by Cambridge University Press

with γ_1/R_1. The voltage potential ϕ is scaled by ϕ_0 (which will be defined later), the ion concentration $n^{(\pm)}$ with n_1^0 (the electroneutral concentration corresponding to ϕ^0), the surface conductivity σ_{si} is scaled with $F\omega_{si}e\Gamma_{mi}$, the surface species $\Gamma_i^{(\pm)}$ on the maximum packing concentration Γ_{mi}, volumetric charge density ρ_i^e on $2n_1^0F$, surface charge q_i with $2\Gamma_{mi}F$ and the conductivity σ_i with $F\omega_i e n_1^0$. Here $F = N_A e$ is the Faraday constant, e is the charge on an electron, N_A is Avogadro's number, ω_i is the ion mobility in the bulk and ω_{si} is the ion mobility at the interfaces. Typically $K_BT/e = 25$ mv (where K_B is Boltzman's constant and T is the temperature) and $\varepsilon_2/\varepsilon_3 \approx 80$ for water and air.

Electrical effects are governed by the equations of electrostatics arising from Maxwell's equations for the electric field, $\boldsymbol{E}_i = -\boldsymbol{\nabla}\phi_i$, in the absence of magnetic fields:

$$\frac{1}{r}\frac{\partial}{\partial r}\left(r\frac{\partial \phi_i}{\partial r}\right) + \delta^2\frac{\partial^2\phi_i}{\partial z^2} = -\frac{1}{\varepsilon_i}\chi^2\rho_i^e, \tag{2.1}$$

where ρ_i^e is the volume charge density in each fluid defined as

$$\rho_i^e = \tfrac{1}{2}(n_i^{(+)} - n_i^{(-)}) \tag{2.2}$$

and $\rho_3^e = 0$ since region 3 is a dielectric. The dimensionless parameter χ represents a ratio of layer thickness to Debye length as

$$\chi^2 = \frac{2R_1^2Fn_1^0}{\phi_0\varepsilon_0}, \tag{2.3}$$

where ε_0 is the permittivity of free space.

At the interfaces, S_1 and S_2, the jump conditions for the electric field are expressed as

$$\varepsilon_1(\phi_{1r} - \delta^2 S_{1z}\phi_{1z}) - \varepsilon_2(\phi_{2r} - \delta^2 S_{1z}\phi_{2z}) = \chi^2\xi_1 q_1\sqrt{1+\delta^2 S_{1z}^2}, \tag{2.4}$$

$$S_{1z}\phi_{1r} + \phi_{1z} = S_{1z}\phi_{2r} + \phi_{2z}, \tag{2.5}$$

$$\varepsilon_2(\phi_{2r} - \delta^2 S_{2z}\phi_{2z}) - \varepsilon_3(\phi_{3r} - \delta^2 S_{2z}\phi_{3z}) = \chi^2\xi_2 q_2\sqrt{1+\delta^2 S_{2z}^2}, \tag{2.6}$$

$$S_{2z}\phi_{2r} + \phi_{2z} = S_{2z}\phi_{3r} + \phi_{3z}, \tag{2.7}$$

with $\xi_i = \Gamma_{mi}/n_1^0R_1$, relating surface species at the interface to electrolyte concentration in the core, $q_i = (\Gamma_i^{(+)} - \Gamma_i^{(-)})/2$ is the surface charge density and the subscripts represent derivatives.

The ionic concentrations, in the core, evolve according to the Nernst–Planck equations:

$$Pe_i\frac{\mathrm{D}n_i}{\mathrm{D}t} = \boldsymbol{\nabla}\cdot(\boldsymbol{\nabla}n_i) - Da_i(n_i - Kn_i^{(+)}n_i^{(-)}), \tag{2.8}$$

for the neutral species and for the ionic species

$$Pe_i(n_{it}^{(\pm)} + u_i n_{ir}^{(\pm)} + w_i n_{iz}^{(\pm)}) = \frac{1}{r}\frac{\partial}{\partial r}(\pm r\psi n_i^{(\pm)}\phi_{ir} + r n_{ir}^{(\pm)})$$
$$+ \delta^2\frac{\partial}{\partial z}(\pm\psi n_i^{(\pm)}\phi_{iz} + n_{iz}^{(\pm)}) + Da_i(n_i - Kn_i^{(+)}n_i^{(-)}), \tag{2.9}$$

where $\psi = \phi_0 e/K_BT$ is a dimensionless field strength. The reaction terms arise from a kinetic model of the disassociation and association of the ions, with rates α_1, α_2,

https://doi.org/10.1017/jfm.2012.145 Published online by Cambridge University Press

respectively and $K = \alpha_2 n_1^0/\alpha_1$ is a ratio of disassociation to association rates (see Saville 1997). The other dimensionless groups appearing above are the Péclet and Damköhler numbers given by

$$Pe_i = \frac{\gamma_1 R_1}{k_B T \mu_1 \omega_i}, \quad Da_i = \frac{R_1^2 \alpha_1}{k_B T \omega_i}, \tag{2.10}$$

which represent the ratio of flow to diffusional (due to charge) velocity scales, and the ratio of diffusion to reaction time scales, respectively.

Applying the electrolyte concentration at the interface, a surface species evolves according to

$$\begin{aligned} &\Gamma_{it}^{(\pm)} + \frac{1}{S_i\sqrt{1+\delta^2 S_{iz}^2}}\frac{\partial}{\partial z}\left(\frac{S_i\Gamma_i^{(\pm)}(w_i + \delta^2 u_i S_{iz})}{\sqrt{1+\delta^2 S_{iz}^2}}\right) \\ &\quad + \frac{\Gamma_i^{(\pm)}(u_i - w_i S_{iz})}{(1+\delta^2 S_{iz}^2)^2}\left(\frac{1+\delta^2 S_{iz}^2}{S_i} - \delta^2 S_{izz}\right) - \frac{\delta^2 S_{it} S_{iz}\Gamma_{iz}^{(\pm)}}{1+\delta^2 S_{iz}^2} \\ &\quad = \frac{Pe_i^{-1}\varpi_i\delta^2}{S_i\sqrt{1+\delta^2 S_{iz}^2}}\frac{\partial}{\partial z}\left(\frac{S_i\Gamma_{iz}^{(\pm)} \pm \psi S_i\Gamma_i^{(\pm)}\phi_{sz}}{\sqrt{1+\delta^2 S_{iz}^2}}\right) + \|J_i \cdot \boldsymbol{n}\| \end{aligned} \tag{2.11}$$

where $\varpi = \omega_{si}/\omega_i$ and the transport term for bulk to interface is

$$J_i \cdot \boldsymbol{n} = \frac{\xi_i^{-1} Pe_i^{-1}}{\sqrt{1+\delta^2 S_{iz}^2}}[(n_{ir}^{(\pm)} - \delta^2 S_{iz}^2 n_{iz}^{(\pm)}) \pm \psi n_i^{(\pm)}(\phi_{ir} - \delta^2 S_{iz}^2 \phi_{iz})]. \tag{2.12}$$

At the interface, the transfer between surface and bulk concentration, $n_i^{(\pm)}$, is governed by a kinetic expression (Davies & Rideal 1961; Prosser & Frances 2001) but we assume that this process is fast relative to diffusive transport to the interface. Also, a reaction term has been ignored for small Damköhler numbers. The vector $\boldsymbol{n}_i = (1, -S_{iz})/(1+S_{iz}^2)^{1/2}$ is the unit normal (pointing outwards) at any point on the interface and $\|(\cdot)\|$ denotes the jump in $(\cdot)$ across the interface, that is, $(\cdot)_2 - (\cdot)_1$ and $(\cdot)_3 - (\cdot)_2$.

The momentum and continuity equations in each layer are given by

$$Re_i\left(\frac{\partial u_i}{\partial t} + u_i\frac{\partial u_i}{\partial r} + w_i\frac{\partial u_i}{\partial z}\right) = -\frac{\partial p_i}{\partial r} - Q\psi^2\chi^2\rho_i^e\frac{\partial \phi_i}{\partial r} + m_i\left(\nabla^2 u_i - \frac{u_i}{r^2}\right), \tag{2.13}$$

$$Re_i\left(\frac{\partial w_i}{\partial t} + u_i\frac{\partial w_i}{\partial r} + w_i\frac{\partial w_i}{\partial z}\right) = -\delta^2\frac{\partial p_i}{\partial z} - \delta^2\psi^2 Q\chi^2\rho_i^e\frac{\partial \phi_i}{\partial z} + m_i\nabla^2 w_i, \tag{2.14}$$

$$\frac{1}{r}\frac{\partial}{\partial r}(r u_i) + \frac{\partial w_i}{\partial z} = 0, \tag{2.15}$$

where the second term on the right-hand side is Maxwell's stress and ∇^2 is the Laplacian. We note that the electrokinetic term in the third layer is negligible, and it is essentially a dielectric. Here, the dimensionless groups appearing in the momentum equation are

$$Re_i = \frac{\rho_i\gamma_1 R_1}{\mu_1^2}, \quad m_i = \frac{\mu_i}{\mu_1}, \quad Q = \frac{\varepsilon_0 (k_B T/e)^2}{R_1\gamma_1} \tag{2.16}$$

and represent the Reynolds number, viscosity ratio and electrostatic Weber number, for electrostatic to capillary pressure, respectively. At the interface, the normal and

https://doi.org/10.1017/jfm.2012.145 Published online by Cambridge University Press

tangential stress balances are

$$-\left\|p_i - \frac{2\,m_i}{1+\delta^2 S_{iz}^2}(u_{ir} - \delta S_{iz}(\delta u_{iz} + \delta^{-1} w_{ir}) + \delta^2 S_{iz}^2 w_{iz})\right\| + \left\|\psi^2 \varepsilon_i \frac{Q}{2}\frac{1-\delta^2 S_{iz}^2}{1+\delta^2 S_{iz}^2}((\phi_{ir})^2 - \delta^2(\phi_{iz})^2) - \varepsilon_i \frac{2\delta^2\psi^2 Q S_{iz}}{1+\delta^2 S_{iz}^2}\phi_{ir}\phi_{iz}\right\| = \gamma_i \kappa_i$$
$$= \gamma_i \left(\frac{1}{S_i\,(1+\delta^2 S_{iz}^2)^{1/2}} - \delta^2 \frac{S_{izz}}{(1+\delta^2 S_{iz}^2)^{3/2}}\right), \tag{2.17}$$

$$\left\|m_i\left(u_{ir}S_{iz} + \frac{1}{2}(1-\delta^2 S_{iz}^2)(u_{iz} + \delta^{-2} w_{ir}) - S_{iz} w_{iz}\right)\right\| = \xi_i \psi^2 \chi^2 Q q_i\,(\phi_i|_{S_i})_z \tag{2.18}$$

with $\gamma_1 = 1$, $\gamma_2 = \gamma_2$ and note that the fluid stress from layer 3 is negligible compared with the viscous fluids. Here $\kappa_i = \nabla \cdot \boldsymbol{n}_i$ is the curvature of the interface. Finally, the dimensionless kinematic condition is

$$S_{it} + w_i S_{iz} = u_i. \tag{2.19}$$

2.2. *Asymptotic reduction*

We make the long-wave assumption by setting $\delta \ll 1$ and adopt expansions of the form $u_i = u_{i0} + \delta^2 u_{i1} + \cdots$, and a similar form for the other variables. For the fluid dynamic parameters we follow Craster *et al.* (2005) and set $Re_1 = \delta^2 \bar{Re}_1$, $Re_2 = \delta^4 \bar{Re}_2$ and $m_2 = \delta^2 M$. Following Conroy *et al.* (2010) we set $Pe_i = \delta^2 \bar{Pe}_i$, $\varpi \sim \delta^2$ and $Da_i = \delta^2 \bar{Da}_i$.

To leading order the electrostatics in each layer is determined from

$$\frac{1}{r}\frac{\partial}{\partial r}\left(r\frac{\partial \phi_{i0}}{\partial r}\right) = -\frac{\chi^2}{\varepsilon_i}\rho_{i0}^e \tag{2.20}$$

$$\frac{\varepsilon_1}{\varepsilon_2}\phi_{10r} - \phi_{20r} = \frac{\chi^2 \xi_1}{\varepsilon_2} q_{10}, \quad \phi_{10} = \phi_{20}, \quad r = S_1 \tag{2.21}$$

$$\phi_{20r} - \frac{\varepsilon_3}{\varepsilon_2}\phi_{30r} = \frac{\chi^2 \xi_2}{\varepsilon_2} q_{20}, \quad \phi_{20} = \phi_{30}, \quad r = S_2. \tag{2.22}$$

Note that the tangential jump condition on the electric field at the interfaces is equivalent to a continuity of potential. The transport of ions is dominated by radial diffusion in each layer

$$\frac{1}{r}\frac{\partial}{\partial r}(\pm\psi r n_{i0}^{(\pm)}\phi_{i0r} + r n_{i0r}^{(\pm)}) = 0 \tag{2.23}$$

$$\frac{1}{r}\frac{\partial}{\partial r}(r\psi\sigma_{i0}\phi_{i0r} + 2r\rho_{i0r}^e) = 0 \tag{2.24}$$

$$\frac{1}{r}\frac{\partial}{\partial r}(2r\psi\rho_{i0}^e\phi_{i0r} + r\sigma_{i0r}) = 0. \tag{2.25}$$

where the last two equations are for the volumetric charge density and conductivity ($\sigma_i = n_i^+ + n_i^-$) that are obtained by subtracting and adding the positive and negative parts of (2.23). We note that these equations are valid for any symmetric electrolyte regardless of the relative ionic mobilities as long as the Péclet numbers are sufficiently small. At the interfaces the surface species, surface charge and surface conductivity

https://doi.org/10.1017/jfm.2012.145 Published online by Cambridge University Press

evolve according to

$$\Gamma_{i0t}^{(\pm)} + (w_{i0}\Gamma_{i0}^{(\pm)})_z + \Gamma_{i0}^{(\pm)} u_{i0} S_{i0}^{-1} = \delta^{-2} \| \xi_i^{-1} \bar{Pe}_i^{-1} (n_{i0r}^{(\pm)} \pm \psi n_{i0}^{(\pm)} \phi_{i0r}) \|, \tag{2.26}$$

$$q_{i0t} + (w_{i0} q_{i0})_z + q_{i0} u_{i0} S_{i0}^{-1} = \delta^{-2} \| \xi_i^{-1} \bar{Pe}_i^{-1} (2\rho_{i0r}^{e} + \psi \sigma_{i0} \phi_{i0r}) \|, \tag{2.27}$$

$$\sigma_{si0t} + (w_{i0}\sigma_{si0})_z + \sigma_{si0} u_{i0} S_{i0}^{-1} = \delta^{-2} \| \xi_i^{-1} \bar{Pe}_i^{-1} (\sigma_{i0r} + 2\psi \phi_{i0r} \rho_{i0}^{e}) \|. \tag{2.28}$$

Assuming that we can express $\rho_i^e \partial\phi_i/\partial r = -\partial\Omega_i/\partial r$ (and similarly for z) and define Ω_i later in the analysis, the leading order radial and axial components of the momentum equation in layer 2 are

$$\frac{\partial P_{20}}{\partial r} = Q\psi^2\chi^2 \frac{\partial \Omega_{20}}{\partial r}, \tag{2.29}$$

$$\frac{\partial P_{20}}{\partial z} = Q\psi^2\chi^2 \frac{\partial \Omega_{20}}{\partial z} + Mr^{-1} (r w_{20r})_r . \tag{2.30}$$

Integrating the first equation the modified pressure $P_{20} - Q\psi^2\chi^2\Omega_{20} = K_2(z,t)$ is independent of r and integrating (2.30) gives

$$w_{20} = \tfrac{1}{4} K_{2z} r^2 M^{-1} + c_1(z,t)\ln(r) + c_2(z,t). \tag{2.31}$$

From the continuity equation the radial velocity is

$$u_{20} = -\tfrac{1}{16} K_{2zz} r^3 M^{-1} - \tfrac{1}{2} r c_{2z} - \tfrac{1}{2} c_{1z} r(\ln(r) - \tfrac{1}{2}) + r^{-1} c_3(z,t). \tag{2.32}$$

At the interface $r = S_2$ the normal and tangential stress balances to leading order are

$$P_{20}|_{S_2} = \gamma_2\kappa_2 + \psi^2 \frac{Q}{2} (\varepsilon_2 (\phi_{20r})^2 - \varepsilon_3 (\phi_{30r})^2)|_{S_2}, \tag{2.33}$$

$$w_{20r}|_{S_2} = -2M^{-1}\xi_2\psi^2\chi^2 Q q_{20} (\phi_{20}|_{S_2})_z . \tag{2.34}$$

From the normal stress balance the constant K_2 is

$$K_2 = \gamma_2\kappa_2 + \psi^2 \frac{Q}{2} (\varepsilon_2 (\phi_{20r})^2 - \varepsilon_3 (\phi_{30r})^2)|_{S_2} - Q\psi^2\chi^2\Omega_{20}|_{S_2} \tag{2.35}$$

and from the tangential stress

$$c_1 = -\frac{S_{20}^2}{2} M^{-1} K_{2z} - 2M^{-1}\xi_2\psi^2\chi^2 Q S_{20} q_{20} (\phi_{20}|_{S_2})_z . \tag{2.36}$$

The other two constants are found from continuity of velocity at $r = S_1$.

To leading order the axial and radial components of the momentum equation in layer 1 are

$$\frac{\partial P_{10}}{\partial r} = Q\psi^2\chi^2 \frac{\partial \Omega_{10}}{\partial r} + \frac{\partial^2 u_{10}}{\partial r^2} + \frac{1}{r}\frac{\partial u_{10}}{\partial r} - \frac{u_{10}}{r^2}, \tag{2.37}$$

$$r^{-1} (r w_{10r})_r = 0. \tag{2.38}$$

From boundedness the second of these yields $w_{10} = w_{10}(z,t)$ and is combined with continuity to obtain the radial component of velocity $u_{10} = -r w_{10z}/2$. The velocity part of the radial component cancel and upon integration the pressure is $P_{10} - Q\psi^2\chi^2\Omega_{10} = K_1(z,t)$. The normal and tangential stress balance at $r = S_1$ is

$$P_{10}|_{S_1} = P_{20}|_{S_1} - w_{10z}|_{S_1} + \psi^2 \frac{Q}{2} [\varepsilon_1 (\phi_{10r})^2 - \varepsilon_2 (\phi_{20r})^2]|_{S_1} + \kappa_1 \tag{2.39}$$

$$w_{10r} = 0. \tag{2.40}$$

https://doi.org/10.1017/jfm.2012.145 Published online by Cambridge University Press

Then from the normal component of the above, the constant of integration is

$$K_1 = K_2 - w_{10z}|_{S_1} + \kappa_1 + Q\chi^2\psi^2(\Omega_{20}|_{S_1} - \Omega_{10}|_{S_1}) + \psi^2\frac{Q}{2}[\varepsilon_1\,(\phi_{10r})^2 - \varepsilon_2\,(\phi_{20r})^2]|_{S_1}. \tag{2.41}$$

From continuity of velocity at $r = S_1$ the remaining constants of integration are

$$c_2 = w_{10}|_{S_1} - \frac{1}{2}K_{2z}M^{-1}\left(\frac{1}{2}S_1^2\right) - c_1\ln(S_1), \tag{2.42}$$

$$c_3 = -\frac{S_1^2}{2}w_{10z}|_{S_1} + \frac{1}{16}K_{2zz}S_1^4M^{-1} + \frac{1}{2}S_1^2c_{2z} + \frac{1}{2}c_{1z}S_1^2\left(\ln(S_1) - \frac{1}{2}\right). \tag{2.43}$$

The leading order axial velocity in the core fluid is determined from the next order in the asymptotic expansion

$$\bar{Re}(w_{10t} + w_{10}w_{10z}) - w_{10zz} + K_{1z} = r^{-1}\,(rw_{11r})_r\,. \tag{2.44}$$

Since the left-hand side of this equation is independent of r we can integrate to obtain

$$w_{11} = \frac{r^2}{4}(\bar{Re}(w_{10t} + w_{10}w_{10z}) - w_{10zz} + K_{1z}) + A(z,t). \tag{2.45}$$

Combining this equation with the next order tangential stress balance at $r = S_1$

$$w_{11r} - Mw_{20r} + u_{10z} + 2S_{10z}(u_{10r} - w_{10z}) = -2\xi_1\psi^2\chi^2Qq_{10}\,(\phi_{10}|_{S_1})_z \tag{2.46}$$

the evolution equation for the axial velocity, combining (2.45)–(2.46), in the core is

$$\begin{aligned}\bar{Re}(w_{10t} + w_{10}w_{10z}) - \frac{3}{S_1^2}\left(S_1^2w_{10z}\right)_z + \kappa_{1z} + \gamma_2\kappa_{2z}\left(\frac{S_2}{S_1}\right)^2 \\ = -\left[Q\chi^2\psi^2(\Omega_{20}|_{S_1} - \Omega_{10}|_{S_1}) + \psi^2\frac{Q}{2}\left(\varepsilon_1\,(\phi_{10r})^2\,|_{S_1} - \varepsilon_2\,(\phi_{20r})^2\right)|_{S_1}\right]_z \\ - \left(\frac{S_2}{S_1}\right)^2\left[\psi^2\frac{Q}{2}\left(\varepsilon_2\,(\phi_{20r})^2\,|_{S_2} - \varepsilon_3\,(\phi_{30r})^2\,|_{S_2}\right) - Q\psi^2\chi^2\Omega_{20}|_{S_2}\right]_z \\ - 4S_1^{-1}\psi^2\chi^2Q\left(\frac{S_2}{S_1}\xi_2q_{20}\,(\phi_{20}|_{S_2})_z + \xi_1q_{10}\,(\phi_{10}|_{S_1})_z\right).\end{aligned} \tag{2.47}$$

Finally the kinematic conditions at the interface are

$$S_{1t} + w_{10}S_{1z} + \frac{S_1}{2}w_{1z} = 0, \tag{2.48}$$

$$S_{2t} + w_2S_{2z} = u_2. \tag{2.49}$$

In the following sections we examine two limits, corresponding to a case where electrokinetic effects are dominant and the other where the equations reduce to the leaky-dielectric model. In general, these two limits depend on the magnitude of the interfacial radii relative to the Debye screening length. For strong electrolytes (e.g. salt concentrations of 1×10^{-3} M or higher) the Debye screening length is typically 10 nm, whereas for weak electrolytes the screening length is between 10 nm and 1 μm (Chang & Yeo 2010). For electrokinetic effects to be important we then need $\chi \sim O(1)$, whereas for a leaky-dielectric model $\chi \gg 1$. In addition, an assumption needs to be made about the relative strength of the surface charge

https://doi.org/10.1017/jfm.2012.145 Published online by Cambridge University Press

relative to the charge in the bulk. For charged surfactants, the adsorption isotherm can be approximated from Borwankar & Wasan (1988) as $\Gamma^{(\pm)} \sim \Gamma_m K_L n^{(\pm)}$ and the relative charge strength as $\Gamma^{(\pm)}/n^{(\pm)}R_0 \sim \Gamma_m K_L/R_0$. For surfactants, Γ_m typically ranges from 1×10^{-6}–1×10^{-5} mol m^{-2} and K_L ranges from 1×10^{-3}–1×10^{7} m^3 mol^{-1} (Chang & Franses 1995). In the systems examined here, we expect the amount of surface-adsorbed ions to be smaller than for surfactants, which have a higher surface affinity, but for the smallest parameters given here we expect the surface charge relative to the bulk (essentially, our dimensionless group ξ_i) to be small for $R \gg 1$ nm. On the other hand, for strong surface affinity we expect the surface charge to play an important role. Further, the strength of the surface charge depends on the adsorption time, $\tau_{ad} \sim 1/k_{ad}n^{(\pm)}$ (where k_{ad} is the rate constant for adsorption), relative to the charge relaxation time, $\tau_r \sim \varepsilon_i/\sigma_i$, and the hydrodynamic time $\tau_{hyd} \sim R_1\mu_1/\gamma_1$. For an air–water system $\tau_{hyd} \sim R_1/100$ s, $\tau_r \sim 1 \times 10^{-8}$ s for strong electrolytes and $\tau_{ad} \sim 0.1$ s (using $k_{ad} = 20$ m^3 mol^{-1} s^{-1} from Borwankar & Wasan 1986). Based on these estimates of the relevant time scales, and since we are interested in time-varying solutions featuring thread breakup, it is possible for us to neglect charge effects by taking $\xi_i \sim O(1)$ and setting $q_i \sim 0$.

2.3. *First limit: weak adsorption*

Assuming the species flux to the interface or the rate of absorption onto the interface is small, we set $\xi_i \sim \delta^2$. In this limit the flux of ions is continuous at both interfaces from (2.26). Further take $\psi = 1$ so that the potential is scaled on k_BT/e, following Conroy *et al.* (2010). Owing to boundedness at $r = 0$ and no flux into layer 3, the ion concentrations in layers 1 and 2 are given by

$$n_{i0}^{(\pm)} = C_i \exp(\mp\phi_{i0}) = n_i^0 \exp(\mp\phi_{i0} \pm \phi_i^0), \tag{2.50}$$

where $n_i^0 = 1$. The constant C_i is determined by assuming the concentration of ions at an electro-neutral state n_i^0 occurs at a potential ϕ_i^0 and that this value depends on the properties of the material. Assuming $\phi_{i0} \ll 1$, with $\phi_i^0 = 0$, the volumetric charge density is $\rho_i^e = -\phi_{i0}n_i^0$. We note that for asymmetric electrolytes the volumetric charge density would also have a linear form in the small potential limit. In this case the equations presented below will have a similar form after a suitable transformation for the potential. The potential in layers 1 and 2 are found from

$$\frac{1}{r}\frac{\partial}{\partial r}\left(r\frac{\partial\phi_{i0}}{\partial r}\right) = \frac{1}{\varepsilon_i}\chi^2 n_i^0\phi_{i0} = \chi_i^2\phi_{i0}, \tag{2.51}$$

with $\chi_3 = 0$ and the interfacial conditions

$$\varepsilon_1\phi_{10r} = \varepsilon_2\phi_{20r}, \quad \phi_{10} = \phi_{20}, \quad r = S_1, \tag{2.52}$$

$$\varepsilon_2\phi_{20r} = \varepsilon_3\phi_{30r}, \quad \phi_{20} = \phi_{30}, \quad r = S_2. \tag{2.53}$$

The solution to (2.51) with the use of the boundary conditions is

$$\phi_{10} = B_2(K_0(\chi_2 S_1) - DI_0(\chi_2 S_1))\frac{I_0(\chi_1 r)}{I_0(\chi_1 S_1)}, \tag{2.54}$$

$$\phi_{20} = B_2(K_0(\chi_2 r) - DI_0(\chi_2 r)), \tag{2.55}$$

$$\phi_{30} = \phi_w + (B_2K_0(\chi_2 S_2) - B_2DI_0(\chi_2 S_2) - \phi_w)\left(\frac{\ln(r/R_3)}{\ln(S_2/R_3)}\right), \tag{2.56}$$

https://doi.org/10.1017/jfm.2012.145 Published online by Cambridge University Press

$$D = \frac{\dfrac{K_0(\chi_2 S_1)}{I_0(\chi_1 S_1)} + \dfrac{\chi_2 \varepsilon_2}{\chi_1 \varepsilon_1}\dfrac{K_1(\chi_2 S_1)}{I_1(\chi_1 S_1)}}{\dfrac{I_0(\chi_2 S_1)}{I_0(\chi_1 S_1)} - \dfrac{\chi_2 \varepsilon_2}{\chi_1 \varepsilon_1}\dfrac{I_1(\chi_2 S_1)}{I_1(\chi_1 S_1)}}, \tag{2.57}$$

$$B_2 = \frac{\phi_w}{\dfrac{\varepsilon_2}{\varepsilon_3}\chi_2 S_2 \ln(S_2/R_3)(DI_1(\chi_2 S_2) + K_1(\chi_2 S_2)) + (K_0(\chi_2 S_2) - DI_0(\chi_2 S_2))}. \tag{2.58}$$

We note that it is possible to solve (2.20) for large potentials provided that the Debye layers are very thin, such that $\chi_i \ll 1$ (Chang & Yeo 2010). Alternatively the potential can be found numerically but we expect the solutions to be qualitatively similar as found in Conroy *et al.* (2010).

Here $\Omega_{i0} = n_i^0 \phi_{i0}^2/2$ and the constants K_2 and c_1 in fluid 2 at $r = S_2$, making use of the interfacial conditions for the derivatives, reduce to

$$K_2 = \gamma_2 \kappa_2 + \bar{Q}\left((\phi_{20r}|_{S_2})^2\left(1 - \frac{\varepsilon_2}{\varepsilon_3}\right) - \chi_2^2 \phi_{20}^2|_{S_2}\right), \tag{2.59}$$

$$c_1 = -\frac{S_{20}^2}{2} M^{-1} K_{2z}, \tag{2.60}$$

where $\bar{Q} = Q\varepsilon_2/2$. In (2.59) the second term represents the electrostatic force from the normal stress component and the third term is the electrokinetic force due to free charges in the bulk.

The evolution equation for the axial velocity at $r = S_1$ is found from the solution to

$$\begin{aligned}\bar{Re}(w_{10t} + w_{10}w_{10z}) - \frac{3}{S_1^2}(S_1^2 w_{10z})_z + \kappa_{1z} + \gamma_2 \kappa_{2z}\left(\frac{S_2}{S_1}\right)^2 \\ = -\bar{Q}\left[\chi_2^2\left(1 - \frac{\varepsilon_1 \chi_1}{\varepsilon_2 \chi_2}\right)\phi_{20}^2|_{S_1} - (\phi_{20r}|_{S_1})^2\left(1 - \frac{\varepsilon_2}{\varepsilon_1}\right)\right]_z \\ - \bar{Q}\left(\frac{S_2}{S_1}\right)^2\left[(\phi_{20r}|_{S_2})^2\left(1 - \frac{\varepsilon_2}{\varepsilon_3}\right) - \chi_2^2 \phi_{20}^2|_{S_2}\right]_z,\end{aligned} \tag{2.61}$$

with the kinematic conditions at the interface:

$$S_{1t} + w_{10}S_{1z} + \frac{S_1}{2}w_{1z} = 0, \tag{2.62}$$

$$S_{2t} + w_2 S_{2z} = u_2. \tag{2.63}$$

The first expression on the right-hand side of (2.61) represents the electrokinetic and electrostatic forces coming from interface 1. The second expression represents the effect on interface 1 from electrostatic forces on S_2 and electrokinetics in the annular layer.

2.3.1. *Connection with other models*

By making the viscosity of the core fluid very large we can investigate the flow of a thin film on the outside of a rigid fibre. Following Craster *et al.* (2005) we set $M \ll 1$ so that the interface remains at $S_1 = 1$ and $w_{10} = 0$ for all time. For a very thin film, we rescale as follows: $r = 1/(1 - y\epsilon_h)$ and $S_2 = 1/(1 - h\epsilon_h)$, where $\epsilon_h \ll 1$ and is a small parameter, so that the fibre is located at $y = 0$ and the free interface at $y = h$. In order to balance electrokinetic terms we take $\chi^2 n_{i0}/\varepsilon_i = \bar{\chi}_i^2 \epsilon_h^{-2}$ and $Q\epsilon_2 = \epsilon_h^2 \bar{Q}$.

https://doi.org/10.1017/jfm.2012.145 Published online by Cambridge University Press

The potential then is found from the solution to

$$\frac{\partial^2\phi_{i0}}{\partial y^2} = \bar{\chi}_i^2\phi_{i0} \to \phi_{20}$$

$$= \phi_{10}(S_1)\cosh(\bar{\chi}_2 y) + \frac{\phi_{20}(S_2) - \phi_{10}(S_1)\cosh(\bar{\chi}_2 h)}{\sinh(\bar{\chi}_2 h)}\sinh(\bar{\chi}_2 y) \tag{2.64}$$

with the core assumed to be a perfect conductor such that $\phi_{10} = \phi_w$ is a constant.

The velocities in the film reduce to

$$u_2 \approx \frac{\epsilon_h^3}{6M}(3h^2 h_z K_{2z} + 2h^3 K_{2zz}), \tag{2.65}$$

$$w_2 \approx -\frac{\epsilon_h^2}{2M}h^2 K_{2z}, \tag{2.66}$$

$$K_{2z} \approx -\gamma_2\epsilon_h(h_z + \epsilon^2\, h_{zzz}) + \epsilon_h\frac{\bar{Q}}{2}\left[(\phi_{20y})^2 - \bar{\chi}^2\phi_{20}^2 - \frac{\varepsilon_3}{\varepsilon_2}(\phi_{30y})^2\right]_z, \tag{2.67}$$

$$\frac{M}{\epsilon_h^2}h_t = \frac{1}{3}\left[h^3 K_{2z}\right]_z \tag{2.68}$$

and we set $M = \epsilon_h^3$ and $\epsilon = 1$. This formulation is for a thin film on the outside of a fibre, but as noted by Kalliadasis & Chang (1994) this equation holds equally well for a thin film coating the inside of a cylindrical pipe, in the absence of electric fields, as studied by Hammond (1983). Further, if fluid 3 is also a perfect conductor, then $\phi_{20} = \phi_I$ and the equation of Conroy *et al.* (2010) is recovered. Otherwise the potential at the gas–liquid interface is coupled to the potential in the gas but the structure of the governing film equation will be the same.

On the other hand, in the limit $M_2 \to \infty$, $c_1 = 0$, $c_3 = 0$, $c_2 = w_{10}$, $w_{20} = w_{10}$ and $u_{20} = -rw_{10z}/2$. Further if the annular fluid has the electrical properties of a gas, that is $\chi_2 = 0$, $\varepsilon_2 = \varepsilon_3$ and $\gamma_2 = 0$, the evolution equations become

$$\bar{Re}(w_{10t} + w_{10}w_{10z}) - \frac{3}{S_1^2}\left(S_1^2 w_{10z}\right)_z + \kappa_{1z} + \gamma_2\kappa_{2z}\left(\frac{S_2}{S_1}\right)^2$$

$$= -\bar{Q}\left[\frac{\varepsilon_1}{\varepsilon_2}(\phi_{10r}|_{S_1})^2 - (\phi_{20r}|_{S_1})^2 - \frac{\varepsilon_1\chi_1}{\varepsilon_2}\phi_{10}^2|_{S_1}\right]_z, \tag{2.69}$$

$$S_{it} + w_{10}S_{iz} + \frac{S_i}{2}w_{1z} = 0, \quad (i = 1, 2), \tag{2.70}$$

which is the single electrified jet model investigated by Conroy *et al.* (2011*b*) in the absence of charged surfactant. Finally, for $\bar{Q} = 0$ or $\chi_1 \ll 1$ and $\chi_2 \ll 1$ this model reduces to the electric-free case studied by Craster *et al.* (2005).

2.4. *Second limit: thin Debye layers and a highly conducting core*

In the second limit we reduce the model to the leaky dielectric one with the free charge at the surface, including a tangential electrostatic stress to the charge at the interface. To do this we want the free charge to only be at the interface, which is possible for thin Debye layers extending from the interfaces and requires $\chi^2/\varepsilon_2 = \bar{\chi}^2\delta^{-2}$ (with $\varepsilon_2 \sim \varepsilon_1$). From the electrostatic equation this limit implies that $\rho_{i0}^e \sim O(\delta^2)$ so that the fluid is electroneutral in the bulk. We take $\xi_1 = \xi_2 = \xi$, which effectively moves the different maximum packing concentrations to the initial condition for the charge. At the interface a charge is present provided that $\xi = \delta^2\bar{\xi}$.

https://doi.org/10.1017/jfm.2012.145 Published online by Cambridge University Press

From (2.28) it follows that σ_{i0} is a constant, a value that is chosen such that $\bar{\sigma}_{i0} = \xi^{-1} Pe_i^{-1} \psi \sigma_{i0} \delta^4$. If the core is an imperfect conductor the charge at the interface is initially zero and remains so for all time. Therefore, we take the core to be a perfect conductor with potential ϕ_1, which we set to zero. In addition, we take ϕ_0 to be the wall potential so that $\phi_w = 1$.

The electric field follows from (2.24) as

$$\frac{1}{r}\frac{\partial}{\partial r}\left(r\frac{\partial \phi_{i0}}{\partial r}\right) = 0, \tag{2.71}$$

$$\phi_{20} = \phi_{10}, \quad r = S_1 \tag{2.72}$$

$$\phi_{20r} - \frac{\varepsilon_3}{\varepsilon_2}\phi_{30r} = \hat{\xi} q_{20}, \quad \phi_{20} = \phi_{30}, \quad r = S_2 \tag{2.73}$$

where $\hat{\xi} = \bar{\xi}\,\bar{\chi}^2$. The potentials in the other two layers are

$$\phi_{20} = \phi_1 + A_2 \ln(r/S_1), \tag{2.74}$$

$$\phi_{30} = \phi_w + A_3 \ln(r/R_3), \tag{2.75}$$

$$A_3 = \frac{\varepsilon_2}{\varepsilon_3}(A_2 - \hat{\xi} S_2 q_2) \tag{2.76}$$

$$A_2\left(1 - \frac{\varepsilon_2}{\varepsilon_3}\frac{\ln(S_2/R_3)}{\ln(S_2/S_1)}\right) = \frac{\phi_w - \phi_1}{\ln(S_2/S_1)} - \frac{\varepsilon_2}{\varepsilon_3} S_2 \hat{\xi} q_2 \frac{\ln(S_2/R_3)}{\ln(S_2/S_1)} \tag{2.77}$$

and the charge evolves according to

$$q_{20t} + (w_{20} q_{20})_z + q_{20} u_{20} S_{20}^{-1} = \bar{\sigma}_{30}\phi_{30r}|_{S_2} - \bar{\sigma}_{20}\phi_{20r}|_{S_2}. \tag{2.78}$$

Since the bulk is electroneutral, $\Omega_{i0} \sim 0$ and the constants K_2 and c_1 at $r = S_2$ are

$$K_2 = \gamma_2 \kappa_2 + \frac{\tilde{Q}}{2}\left((\phi_{20r}|_{S_2})^2 - \frac{\varepsilon_3}{\varepsilon_2}(\phi_{30r}|_{S_2})^2\right), \tag{2.79}$$

$$c_1 = -\frac{S_{20}^2}{2} M^{-1} K_{2z} - 2M^{-1}\hat{\xi}\tilde{Q} S_{20} q_{20} (\phi_{20}|_{S_2})_z, \tag{2.80}$$

where $\tilde{Q} = Q\psi^2\varepsilon_2$. The velocity in the annular layer is expressed as in (2.31) and (2.32) with the constants c_2 and c_3 found in (2.42) and (2.43). The evolution equation for the axial velocity at $r = S_1$ is

$$\begin{aligned}\bar{Re}(w_{10t} + w_{10} w_{10z}) - \frac{3}{S_1^2}(S_1^2 w_{10z})_z + \kappa_{1z} + \gamma_2 \kappa_{2z}\left(\frac{S_2}{S_1}\right)^2 \\ = \frac{\tilde{Q}}{2}[(\phi_{20r}|_{S_1})^2]_z - \frac{\tilde{Q}}{2}\left(\frac{S_2}{S_1}\right)^2\left[(\phi_{20r}|_{S_2})^2 - \frac{\varepsilon_3}{\varepsilon_2}(\phi_{30r}|_{S_2})^2\right]_z \\ - 4\hat{\xi}\tilde{Q}\left(\frac{S_2}{S_1}\right)^2 (S_2^{-1} q_{20} (\phi_2|_{S_2})_z).\end{aligned} \tag{2.81}$$

Finally the kinematic conditions at the interface are

$$S_{1t} + w_{10} S_{1z} + \frac{S_1}{2} w_{1z} = 0, \tag{2.82}$$

$$S_{2t} + w_2 S_{2z} = u_2. \tag{2.83}$$

https://doi.org/10.1017/jfm.2012.145 Published online by Cambridge University Press

In (2.81) the electrokinetic term has been dropped but we picked up a tangential stress at the interface due to the electrostatic field. We absorb $\hat{\xi}$ by redefining as follows: $q_{20}\hat{\xi} \to q_{20}$ and $\bar{\sigma}_{i0}\hat{\xi} \to \bar{\sigma}_{i0}$.

3. Results

The final system of equations is parameterized by the following dimensionless groups: the Reynolds number, $\bar{Re}$; the ratio of the viscosity of the annular and core fluids, M; the ratio of the surface tension of the annular and core fluids, γ_2; the slenderness parameter, δ; the ratio of the initial annular interface radius to the core, α; the electrode radius, R_3; the dimensionless wall potential, ϕ_w; electric Weber number, $\bar{Q} = Q\varepsilon_2/2$ (and $\tilde{Q} = Q\psi^2\varepsilon_2$); dielectric permittivity, ε_i; scaled inverse Debye length, $\chi_i = \chi\sqrt{n_i^0/\varepsilon_i}$; and conductivity, $\bar{\sigma}_i$.

The hydrodynamic parameters have been explored in Craster *et al.* (2005) so we use a basic case studied by them and focus only on the parameters related to the electric field. That is, $M = 1$, $\gamma_2 = 1$, $\alpha = 1.5$ and $\delta = 0.05$ unless noted otherwise. The effect of ϕ_w on the solution is similar to $\bar{Q}$ so we take $\phi_w = 1$ in the first limit. Typically $\varepsilon_2/\varepsilon_3 = 80$ for an air–water interface so we use that as a base value here. The value of the electrode radius has been set to $R_3 = 10$ so that the viscous fluids do not make contact with the walls and has been used previously (Collins *et al.* 2007; Conroy *et al.* 2011*b*).

3.1. *Linear theory*

We can gain insight into the solution to the governing equations by conducting a linear stability analysis. The results will also act as validation against the numerical solutions for early times. For each case we use the following decomposition

$$(S_1, S_2, w_1, q_i) = (1, \alpha, 0, q_{i0}) + (\hat{S}_1, \hat{S}_2, \hat{w}_1, \hat{q}_i), \tag{3.1}$$

where α is the ratio of outer to inner initial undisturbed positions and hats indicate infinitesimal perturbations. The perturbation of the charge will only be applicable for the second case. In addition, we note that the potential and ion concentrations are effectively expanded through the perturbation of the interfaces, so there is no need to include a decomposition for these variables in (3.1).

3.1.1. *First limit: weak adsorption*

Using the decomposition (3.1), linearization of the kinematic conditions yields

$$\hat{S}_{1t} = -\tfrac{1}{2}\hat{w}_{1z}, \quad \hat{S}_{2t} = \hat{u}_2|_\alpha. \tag{3.2}$$

Since the linearized form of the electric terms have long expressions we prefer to introduce the following $f_i = (\phi_{20r}|_{S_i})^2$ and $g_i = \phi_{20}^2|_{S_i}$ and make a multidimensional Taylor series expansion about the undisturbed state. The velocity at the second interface is

$$\hat{u}_2|_\alpha = -\frac{\alpha}{2}\hat{w}_{1z} + A\hat{K}_{2zz}, \tag{3.3}$$

$$\hat{K}_{2zz} = \frac{-\gamma_2}{\alpha^2}(\hat{S}_{2zz} + \delta^2\alpha^2\hat{S}_{2zzzz}) + \frac{\bar{Q}}{2}\varepsilon_2\left(\left(1 - \frac{\varepsilon_2}{\varepsilon_3}\right)\left(\frac{\partial f_2}{\partial S_1}\hat{S}_{1zz} + \frac{\partial f_2}{\partial S_2}\hat{S}_{2zz}\right) - \chi_2^2\left(\frac{\partial g_2}{\partial S_1}\hat{S}_{1zz} + \frac{\partial g_2}{\partial S2}\hat{S}_{2zz}\right)\right) \tag{3.4}$$

https://doi.org/10.1017/jfm.2012.145 Published online by Cambridge University Press

with $A = (-3\alpha^3/4 + \alpha - \alpha^{-1}/4 + \alpha^3 \ln(\alpha))/4M$ and the velocity at the first interface is

$$\begin{aligned}
&\bar{R}e\hat{w}_{1t} - 3\hat{w}_{1zz} - (\hat{S}_{1z} + \delta^2\hat{S}_{1zzz}) - \gamma_2((\hat{S}_{2z} + \alpha^2\delta^2\hat{S}_{2zzz}) \\
&\quad = -\bar{Q}\left(\chi_2^2\left(1 - \frac{\varepsilon_1\chi_1}{\varepsilon_2\chi_2}\right)\left(\frac{\partial g_1}{\partial S_1}\hat{S}_{1z} + \frac{\partial g_1}{\partial S_2}\hat{S}_{2z}\right) - \left(\frac{\partial f_1}{\partial S_1}\hat{S}_{1z} + \frac{\partial f_1}{\partial S2}\hat{S}_{2z}\right)\left(1 - \frac{\varepsilon_2}{\varepsilon_1}\right)\right) \\
&\qquad - \bar{Q}\alpha^2\left(\left(1 - \frac{\varepsilon_2}{\varepsilon_3}\right)\left(\frac{\partial f_2}{\partial S_1}\hat{S}_{1z} + \frac{\partial f_2}{\partial S_2}\hat{S}_{2z}\right) - \chi_2^2\left(\frac{\partial g_2}{\partial S_1}\hat{S}_{1z} + \frac{\partial g_2}{\partial S2}\hat{S}_{2z}\right)\right). \qquad (3.5)
\end{aligned}$$

Substituting the following normal mode expansion

$$(\hat{S}_1, \hat{S}_2, \hat{w}_1) = (\bar{S}_1, \bar{S}_2, \bar{w}_1)\mathrm{e}^{\lambda t + ikz}, \qquad (3.6)$$

into the above expressions we obtain an eigenvalue equation for the growth rate λ with three roots:

$$\begin{aligned}
&\bar{R}e\lambda^2 + 3k^2\lambda - \frac{k^2}{2}(1 - \delta^2k^2) - \gamma_2\lambda\eta(1 - \delta^2\alpha^2k^2)k^2 \\
&\quad = -\bar{Q}k^2\lambda\left(\chi_2^2\left(1 - \frac{\varepsilon_1\chi_1}{\varepsilon_2\chi_2}\right)\left(\frac{1}{2}\frac{\partial g_1}{\partial S_1} + \eta\lambda\frac{\partial g_1}{\partial S_2}\right) - \left(1 - \frac{\varepsilon_2}{\varepsilon_1}\right)\left(\frac{1}{2}\frac{\partial f_1}{\partial S_1} + \eta\lambda\frac{\partial f_1}{\partial S_2}\right)\right) \\
&\qquad - \bar{Q}\alpha^2k^2\left(\left(1 - \frac{\varepsilon_2}{\varepsilon_3}\right)\left(\frac{1}{2}\frac{\partial f_2}{\partial S_1} + \eta\lambda\frac{\partial f_2}{\partial S_2}\right) - \chi_2^2\left(\frac{1}{2}\frac{\partial g_2}{\partial S_1} + \eta\lambda\frac{\partial g_2}{\partial S_2}\right)\right) \qquad (3.7)
\end{aligned}$$

with the variable η defined as

$$2\eta = \frac{\alpha + \dfrac{A}{\lambda}\bar{Q}k^2\left(\chi_2^2\dfrac{\partial g_2}{\partial S_1} - \left(1 - \dfrac{\varepsilon_2}{\varepsilon_3}\right)\dfrac{\partial f_2}{\partial S_1}\right)}{\lambda + \gamma_2\alpha^{-2}Ak^2(-1 + \delta^2\alpha^2k^2) + A\bar{Q}k^2\left((1 - \varepsilon_2/\varepsilon_3)\dfrac{\partial f_2}{\partial S_2} - \chi_2^2\dfrac{\partial g_2}{\partial S_2}\right)}. \qquad (3.8)$$

Typical dispersion curves, as a function of the electric field parameters, are shown in figure 2 with the stretching and squeezing modes shown on the same figure. In all cases the stretching mode dominates as found in Craster *et al.* (2005) in the absence of electric fields.

In the first set of plots for $\bar{Q}$, shown in figure 2(*a*), the electric field acts to create an effective electric double layer that extends from $r = S_2$ towards the centre and forms a repulsive force that stabilizes the thread. Also, as discussed in Wang, Mahlmann & Papageorgiou (2009), the electric field in the gas layer has a stabilizing effect for long waves and electrode radii that are sufficiently large (as studied here). Therefore, as $\bar{Q}$ increases, the growth rate of the stretching and squeezing modes decrease at all wavenumbers and such an increase has a stabilizing effect. Although the stretching mode is more sensitive than the squeezing mode, it always dominates even for large values of $\bar{Q}$. For very large values of $\bar{Q}$ (not shown here) the electric field completely stabilizes the interfaces. Further, the cutoff wavenumber is unchanged by increasing $\bar{Q}$ for the stretching mode but for the squeezing mode the cutoff wavenumber decreases with increasing $\bar{Q}$.

In figure 2(*b*), showing variations in $\varepsilon_2/\varepsilon_1$, the maximum growth rate for both modes decreases as $\varepsilon_2/\varepsilon_1$ increases. We can gain insight into the reasons for this by looking at the plot of the potential shown in figure 4. Since the compound jet is axisymmetric, a repulsive electric double layer extends from the outer interface, S_2, towards the centreline. As $\varepsilon_2/\varepsilon_1$ decreases, the radial electric field in the core fluid decreases, from the boundary condition $\phi_{10r} = \phi_{20r}\varepsilon_2/\varepsilon_1$, causing destabilization by

https://doi.org/10.1017/jfm.2012.145 Published online by Cambridge University Press

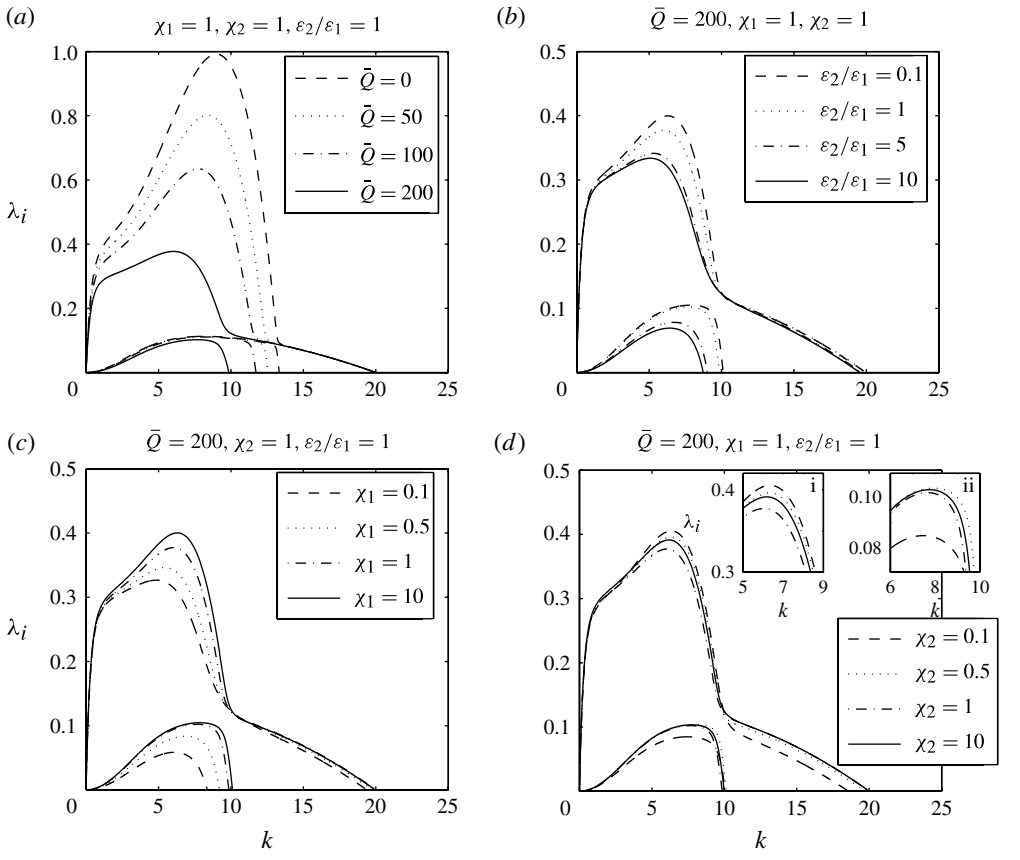


FIGURE 2. Dispersion curves showing the stretching and squeezing modes for the formulation of the first limit. Here $M = 1$, $\gamma_2 = 1$, $\alpha = 1.5$, $\delta = 0.05$, $\phi_w = 1$, $R_3 = 10$ $\varepsilon_2/\varepsilon_3 = 80$ and the other parameter values are listed in the figure. The lines with a smaller value of λ correspond to the squeezing mode whereas the larger curves are for the stretching modes. In (*d*) magnifications (i) and (ii) correspond to the maximum values of the stretching and squeezing modes, respectively.

reducing the repulsive electrokinetic force. Further, the cutoff wavenumber decreases as $\varepsilon_2/\varepsilon_1$ increases for the squeezing mode but the cutoff wavenumber has a non-monotonic behaviour for the stretching mode. At small values of $\varepsilon_2/\varepsilon_1$ the cutoff wavenumber increases with an increase in this ratio and the cutoff wavenumber decreases at large $\varepsilon_2/\varepsilon_1$ for increases in this ratio.

Variations in the Debye lengths χ_i on the dispersion curves are displayed in figure 2(*c*,*d*). In figure 2(*c*) the dispersion curves show a destabilizing effect as the maximum growth rate increases as χ_1 decreases for the stretching and squeezing modes. As χ_1 increases the potential in the core and annular fluid decreases. Also, as χ_1 increases the stabilizing electrokinetic repulsion decreases in strength, as the Debye length decreases and the thread destabilizes. The Debye length χ_1 represents the core radius relative to the distance of charge separation in the core. For small values of χ_1 the Debye length is large relative to the radius and as a consequence of boundedness at $r = 0$ the potential in the core approaches a constant. For large χ_1 the Debye layer is thin and the potential approaches the charge neutral state with $\phi = 0$. Further, for

https://doi.org/10.1017/jfm.2012.145 Published online by Cambridge University Press

the squeezing mode the cutoff wavenumber increases with an increase in χ_1 but has a non-monotonic behaviour for the stretching mode. For small χ_1 the cutoff wavenumber increases with this parameter but for large χ_1 the cutoff wavenumber decreases with this parameter.

The dispersion curves for variations in χ_2 are presented in figure 2(*d*), showing non-monotonic behaviour for $\lambda_1(\max)$ for the stretching and squeezing modes. For small χ_2, $\lambda_1(\max)$ decreases for the squeezing mode and increases for the stretching mode as χ_2 decreases and for large χ_2 this trend reverses. The cutoff wavenumber dependence on χ_2 also show a non-monotonic behaviour. For small χ_2 the cutoff wavenumber decreases for the stretching mode and increases for the squeezing mode as χ_2 increases with this trend reversing for larger values of χ_2. For small χ_2 the Debye layer is large relative to the thickness of the annular fluid and the potential varies logarithmically. For large χ_2 the Debye layer is thin, implying electroneutrality in the annular fluid. Since the potential is continuous, the core is also approximately electroneutral and a Debye layer exists at $r = S_2$.

3.1.2. *Second limit: thin Debye layers and a highly conducting core*

Here we follow a similar procedure as in the first limit and use the normal mode expansion:

$$(S_1, S_2, w_1, q_2) = (1, \alpha, 0, q_{20}) + (\bar{S}_1, \bar{S}_2, \bar{w}_1, \bar{q}_2)\mathrm{e}^{\lambda t + \mathrm{i}kz}, \tag{3.9}$$

where the charge on the interface at steady state is found from (2.78) to be

$$q_{20} = \frac{\phi_w - \phi_1}{\left(\dfrac{\sigma_3\dfrac{\varepsilon_2}{\varepsilon_3}}{\sigma_3\dfrac{\varepsilon_2}{\varepsilon_3} - \sigma_2}\right)\left(\alpha\ln(\alpha) - \alpha\dfrac{\varepsilon_2}{\varepsilon_3}\ln(\alpha/R_3)\right) + \dfrac{\varepsilon_2}{\varepsilon_3}\alpha\ln(\alpha/R_3)}. \tag{3.10}$$

We have left $\bar{\sigma}_3$ in the above expression but this parameter is negligible for a gas so we take $\bar{\sigma}_3 = 0$ later in the analysis. Following the previous section we have four equations corresponding to the interface radii, core axial velocity and charge at the gas liquid interface that are combined to obtain an equation for λ that has four roots. We suppress the form of this equation here but the details can be found in the Appendix. In the limit $\bar{\sigma}_2 \gg 1$, the electric field in the annular fluid satisfies $\phi_{20r}|_{S_2} \ll 1$ from (2.78). The annular fluid, in this case is a perfect conductor and we can express the dispersion relation as

$$\begin{aligned}&\left[\lambda(\lambda\bar{R}_e + 3k^3) - \frac{1}{2}k^2(1 - k^2\delta^2)\right]\\ &\quad\times\left[\lambda - \frac{A_2}{4M}\gamma_2\alpha^{-2}(k^2 - \delta^2\alpha^2k^4) - \frac{A_2}{4M}\left(\frac{\tilde{Q}\phi_w^2\dfrac{\varepsilon_3}{\varepsilon_2}k^2}{\alpha^3}\right)\left(\frac{\ln(\alpha/R_3)+1}{\ln(\alpha/R_3)^3}\right)\right]\\ &\quad= \frac{1}{2}\alpha k^2\lambda\left[\gamma_2(1 - k^2\delta^2\alpha^2) - \left(\frac{\tilde{Q}\phi_w^2\dfrac{\varepsilon_3}{\varepsilon_2}}{\alpha}\right)\left(\frac{\ln(\alpha/R_3)+1}{\ln(\alpha/R_3)^3}\right)\right]\end{aligned} \tag{3.11}$$

which is of a similar form to the dispersion relation for single jets studied in Wang *et al.* (2009). As in the single jet case the electric field will introduce a stabilizing effect for sufficiently large electrode positions. From the dispersion relation (3.11) the

https://doi.org/10.1017/jfm.2012.145 Published online by Cambridge University Press

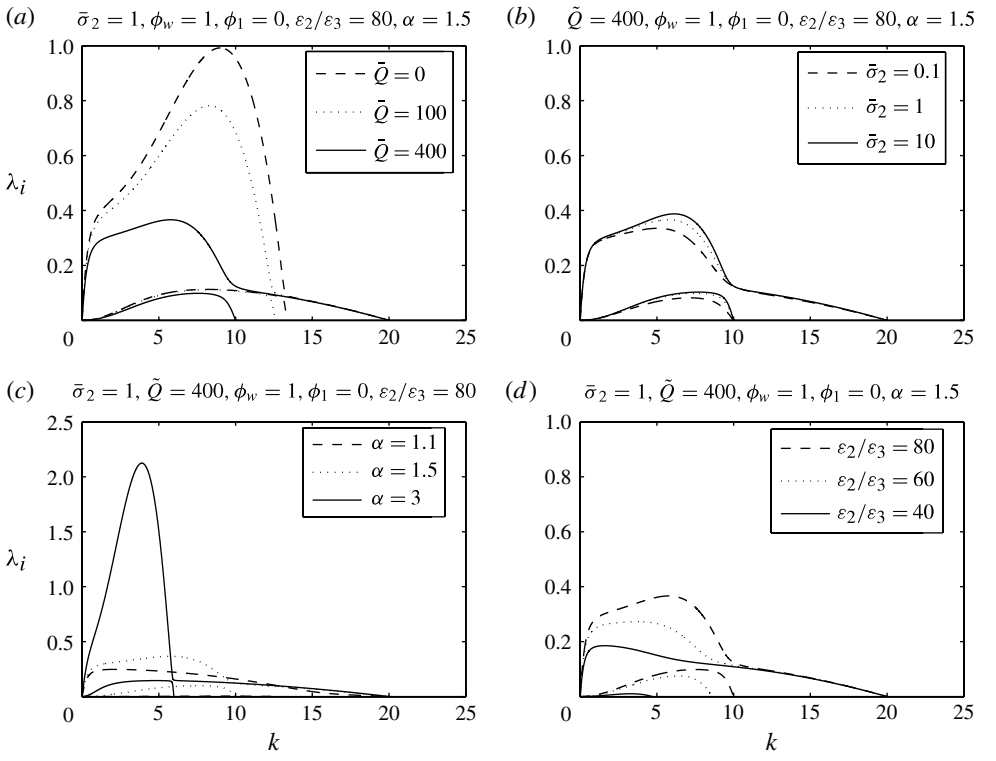


FIGURE 3. Dispersion curves, showing the effect of the electric field on the growth rate of disturbances for the formulation of the second limit. Here $M = 1$, $\gamma_2 = 1$, $\delta = 0.05$, $\phi_w = 1$, $R_3 = 10$ and the other parameter values are listed in the figure. The lines with a smaller value of λ correspond to the squeezing mode whereas the larger curves are for the stretching modes.

electrostatic term changes sign at $R_3 = \alpha \exp(1)$ and has a stabilizing effect for R_3 greater than this value and a destabilizing effect otherwise.

Typical dispersion curves are shown in figure 3. In all figures the larger values of λ correspond to the stretching mode and the smaller curves are the squeezing modes. The electric field has a stabilizing effect; as $\tilde{Q}$ increases λ decreases with the effect being more pronounced for the stretching mode. This result is consistent with compound electrified jets (Li *et al.* 2008) with small wavenumbers and (Wang *et al.* 2009) for single jets, where the most dangerous mode was found to decrease as the electrostatic pressure increases for electrode radii larger than a critical value (given by them to be $R_3 > \exp(1)$). Also, the difference between the maximum value of the squeezing and stretching modes decreases as $\tilde{Q}$ increases since the squeezing mode is less affected by the electric field. The cutoff wavenumber for the stretching mode does not change with $\tilde{Q}$, whereas for the squeezing mode the cutoff wavenumber decreases with $\tilde{Q}$.

The effect of the conductivity $\bar{\sigma}_2$ on the dispersion curves is shown in figure 3(*b*). As $\bar{\sigma}_2$ increases λ increases with no discernible change to the cut-off mode. For large $\bar{\sigma}_2$ the potential in the annular layer approaches the core value, that is $\phi_2 \to \phi_1 = 0$, and the model reduces to that of perfectly conducting coaxial fluids, with the dispersion curve independent of the conductivity. On the other hand as $\bar{\sigma}_2 \to 0$

https://doi.org/10.1017/jfm.2012.145 Published online by Cambridge University Press

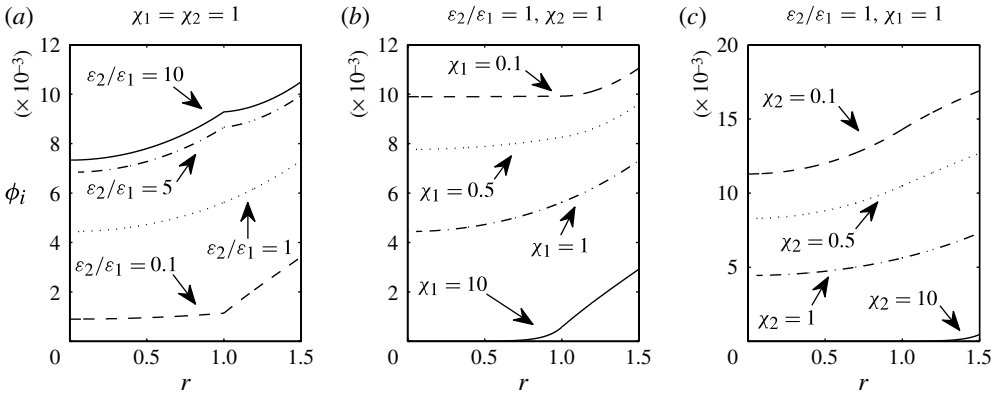


FIGURE 4. Potential in fluids 1 and 2 from (2.54)–(2.55) for $S_1 = 1$, $S_2 = \alpha = 1.5$, $R_3 = 10$ and as a function of the parameters χ_i and $\varepsilon_2/\varepsilon_1$.

the total charge at the interface becomes constant with the dispersion curves also independent of the conductivity. Since the maximum growth rate for finite conductivity is smaller than that for a perfectly conducting fluid, for very large conductivities, the presence of the leaky dielectric fluid as opposed to a perfectly conducting one contributes an added destabilizing effect.

In figure 3(*c*), the dispersion curves are shown for variations in the relative initial fluid thicknesses α. Increasing α results in a reduction of viscous dissipation in the annular region and λ increases. The wavenumber, k, corresponding to the maximum value of λ also increases for small α but decreases for larger α. This result has been attributed, by Craster *et al.* (2005), to a relative increase in resistance to extensional flow in the inner fluid to the resistance to flow in the outer fluid. Further, the effect of $\varepsilon_2/\varepsilon_3$ on the dispersion curves is shown in figure 3(*d*). Decreasing this ratio causes the growth rates to decrease as well as k at the maximum value of λ. We can understand this by looking at solutions for large $\varepsilon_2/\varepsilon_3$. In this case we can express $\phi_{20r} \sim S_2 q_2/r - (\varepsilon_3/\varepsilon_2)/r \ln(S_2/R_3)$ and $\phi_{30r} \sim 1/r \ln(S_2/R_3)$ and therefore increasing ε_2 causes the radial derivative of potential in the annular region to decrease. From the normal Maxwell's stress the effect of $\varepsilon_2/\varepsilon_3$ can then be understood as a modified electric Weber number, of size $\tilde{Q}\,(\varepsilon_3/\varepsilon_2)^2$.

3.2. *Numerical results*

The governing equations are solved numerically on a periodic domain, using a pseudo-spectral method that uses fast Fourier methods for space and Gear's method for time. The initial conditions are given from (3.1) with $\hat{S}_2 = 1 \times 10^{-4}$ and k corresponding to the most dangerous mode. In the simulations 512 nodes are typically used without any noticeable difference in the solutions upon doubling the number of nodes. We have checked that mass is conserved in the numerical results and that the results are consistent with linear theory during the initial stages of thread breakup. The interfacial positions as a function of the parameters that affect the electric field are shown in figures 5–10 for the first limit and figures 12 and 13 for the second limit.

3.2.1. *First limit: weak adsorption*

We first examine the effect of $\bar{Q}$ on the interfacial positions, shown in figure 5. Without electric field effects the annular fluid thins more rapidly than the core, because the viscosity is lower there, and the two interfaces approach each other by a fluid

https://doi.org/10.1017/jfm.2012.145 Published online by Cambridge University Press

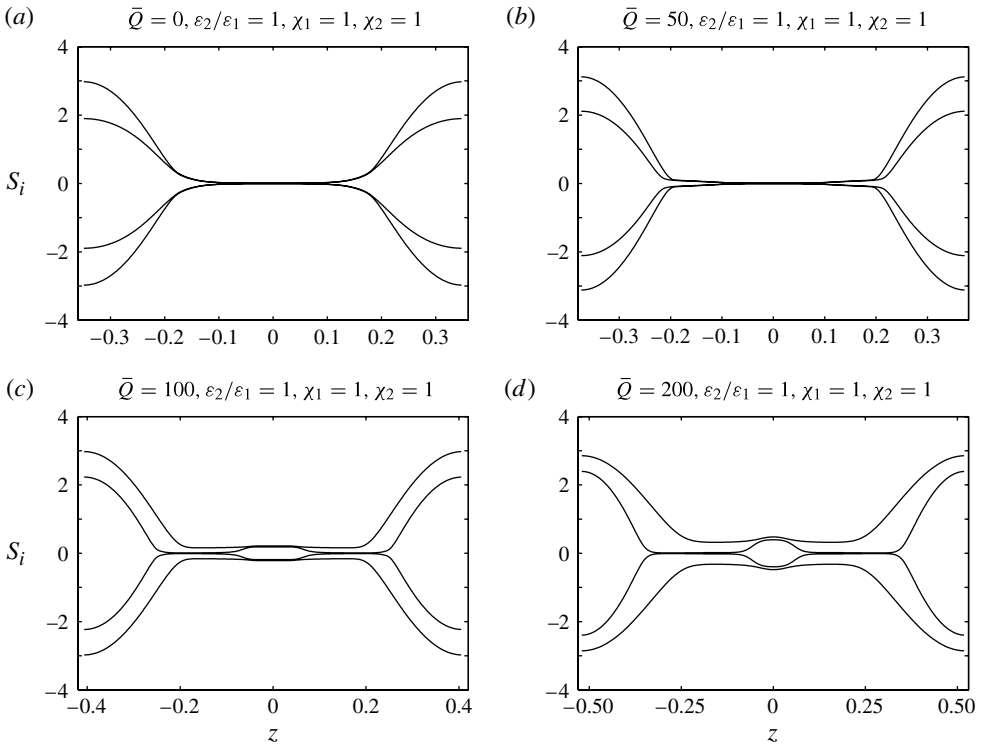


FIGURE 5. Interface radii S_1 and S_2 as a function of $\bar{Q}$ for the formulation of the first limit. Here $M = 1$, $\gamma_2 = 1$, $\alpha = 1.5$, $\delta = 0.05$, $\phi_w = 1$, $R_3 = 10$ $\varepsilon_2/\varepsilon_3 = 80$ and the other parameter values are listed in the figure. The solutions are initiated from the most dangerous mode, which corresponds to $k = 9$ (*a*), 8.4 (*b*), 7.73 (*c*) and 6.04 (*d*). The times associated with these profiles is $t = 17.35$ (*a*), 21.83 (*b*), 26.76 (*c*) and 38.25 (*d*).

drainage process. At the final state both interfaces pinch at $z = 0$, forming only a primary satellite (Craster *et al.* 2005). With electric field effects included the interface evolution slows, due to the stabilizing effect of the electric field, which was indicated by linear theory. For small values of $\bar{Q}$ the interfaces still pinch at $z = 0$ but the shape near this point is less smooth. For sufficiently large values of the electric Weber number $\bar{Q}$ a satellite forms at the centre and grows in size as $\bar{Q}$ increases. From the electrokinetic repulsion in the annular fluid and the electrostatic force arising from the gas, the evolution of interface S_2 is slowed relative to the more viscous core fluid as shown in figure 6. In (*a*) the minimum interface radius of both interfaces is plotted as a function of time, showing that the electric field keeps the two interface separated by some distance that increases with $\bar{Q}$. Since the two interfaces are held apart, the fluid drainage process is reduced and satellite formation in the core is promoted. Although a satellite does not form in the electric free case it does when the viscosities of both fluids are of a comparable value (Craster *et al.* 2003; Suryo *et al.* 2006).

For larger values of $\bar{Q}$, the core fluid forms a satellite, that has a familiar structure to the single-jet problem, although the annular layer thickness is relatively large near the pinch point. In the limit $S_1 \to 0$ the potential in the core is constant in the radial

https://doi.org/10.1017/jfm.2012.145 Published online by Cambridge University Press

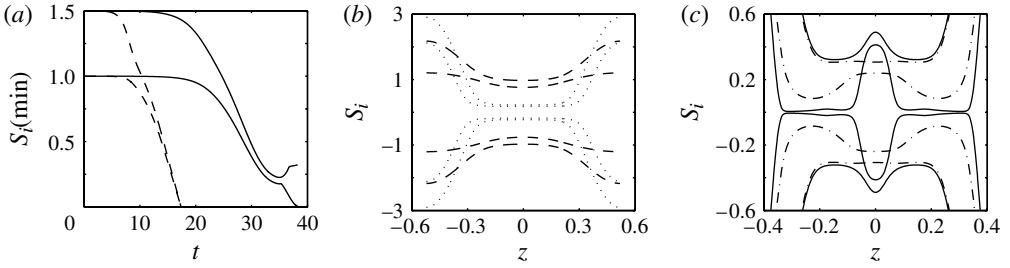


FIGURE 6. (*a*) Minimum interface radius for the electric free case (dashed line) from figure 5(*a*) and inclusion of electric effects (solid line) from figure 5(*d*). (*b*,*c*) Interface radii S_1 and S_2 (corresponding to the solid line in *a*) at $t = 25$ (dashed line), 35 (dotted line), 36.7 (dash-dotted line) and 38.25 (solid line). Here $M = 1$, $\gamma_2 = 1$, $\alpha = 1.5$, $\delta = 0.05$, $\phi_w = 1$, $R_3 = 10$, $\varepsilon_2/\varepsilon_3 = 80$ and $\hat{S}_2 = 1 \times 10^{-4}$.

direction and equal to

$$\phi_1 = \frac{\phi_w}{I_0(S_2\chi_2) - \chi_2 \dfrac{\varepsilon_2}{\varepsilon_3} S_2 \ln\left(\dfrac{S_2}{R_3}\right) I_1(S_2\chi_2)} \tag{3.12}$$

and the potential in the annular layer is $\phi_2 = \phi_1 I_0(\chi_2 r)$. In (2.61) the electric field parameters arising in the core near the pinch point drop out but the electrostatic/electrokinetic terms in the annular layer are present and large due to the term $(S_2/S_1)^2$. At the top of the satellite the annular fluid can be very thin. In the limit $S_1 \to S_2$ ($S_1 \gg 0$) the electric field looks like the thin annular case with the potential having a solution that is similar to (2.64) which is a sum of hyperbolic functions.

The effect of varying $\varepsilon_2/\varepsilon_1$ on the final interface radii is seen in figure 7. For small values of $\varepsilon_2/\varepsilon_1$ the gradient in the potential at $r = S_1$ is weak and the core potential is approximately constant. Here the satellite size and the thickness of the annular layer above the satellite is smaller than the base case shown in (*b*). As $\varepsilon_2/\varepsilon_1$ increases the radius of the satellite increases as well as the annular fluid thickness above the satellite, although less sensitively for larger dielectric permittivity ratios.

Next we turn to the effect of the Debye layer thickness on the interface radii, shown in figures 8–10. The Debye layer relates the thickness of the electric double layer to the thickness of the fluid and defines the electrokinetic force on the system. For small χ_1, shown in figure 8, the Debye layer is thick relative to the interface radius and the potential in the core approaches a constant value. On the other hand for larger χ_1 the Debye layer thickness is very thin and the potential in the core is at the electroneutral value of $\phi_1 = 0$ except near the interface. Further, as χ_1 increases the potential in both layers decreases and as a result, the radius of the satellites and annular layer thickness above the satellites decrease.

For χ_2, shown in figure 9, the behaviour of the system has some similar characteristics to that of the double layer in the core. From linear theory, the maximum growth rate decreases as χ_2 increases for small χ_2. The satellite does not form for small values of χ_2 shown in figure 10. Instead the outer interface undergoes drainage-like dynamics, forming a series of lobes and collars that are more easily seen in the magnification in figure 10(*b*). The outer interface evolves toward the core fluid and is expected to make contact in finite time. If $\bar{Q}$ is increased while fixing χ_2 the interfaces evolve to a stable position displayed in figure 10(*c*), forming a thinner

https://doi.org/10.1017/jfm.2012.145 Published online by Cambridge University Press

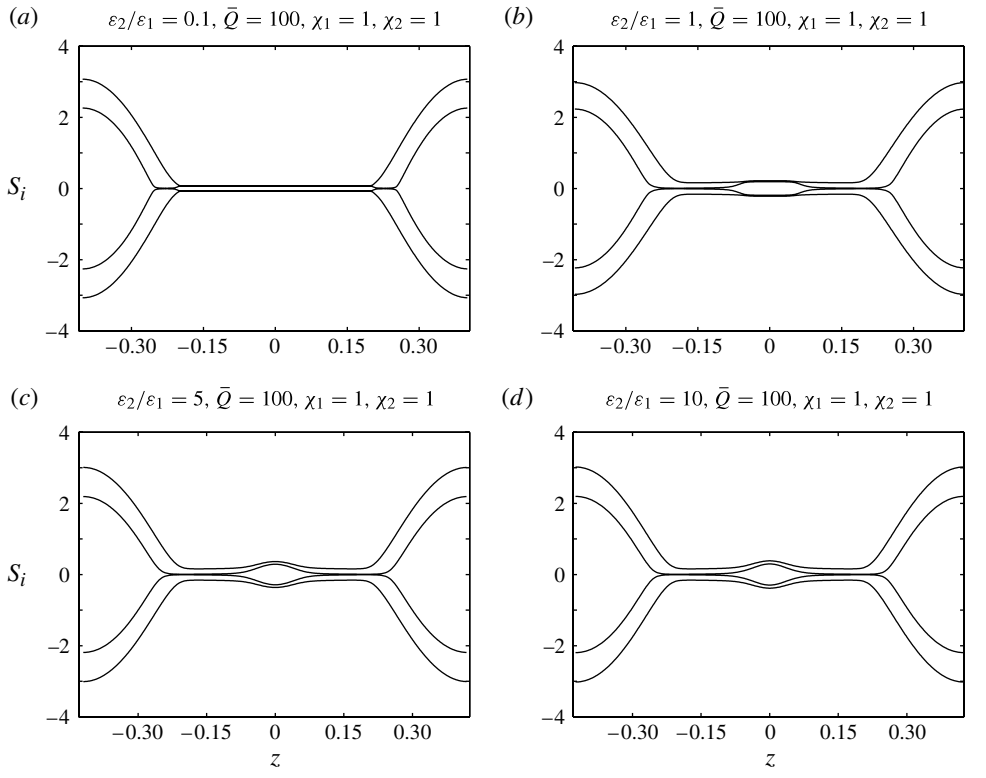


FIGURE 7. Interface radii S_1 and S_2 as a function of $\varepsilon_2/\varepsilon_1$ for the formulation of the first limit. Here $M = 1$, $\gamma_2 = 1$, $\alpha = 1.5$, $\delta = 0.05$, $\phi_w = 1$, $R_3 = 10$, $\varepsilon_2/\varepsilon_3 = 80$ and the other parameter values are listed on the figure. The solutions are initiated from the most dangerous mode, which corresponds to $k = 7.82$ (*a*), 7.73 (*b*), 7.48 (*c*) and 7.4 (*d*). The times associated with these profiles is $t = 25.99$ (*a*), 26.74 (*b*), 27.00 (*c*) and 27.17 (*d*).

compound thread. We have checked numerically that these interface radii are stable to perturbations. As χ_2 increases further, a satellite forms and increases in radius with an increase in χ_2. For large values of χ_2 the double layer thins at $r = S_2$ and causes the potential in the viscous fluids to decrease to low values. As a result, the electrokinetic and electrostatic forces decrease and a satellite does not form.

In figure 11 we have plotted the solution with the initial disturbance generated from uniform random noise on a long domain. As expected the evolution of the interface selects the most dangerous stretching mode $\lambda = 0.6347$ that was predicted by linear theory. In the right-hand figure the evolution of the growth rate is compared against the solution from linear theory showing good agreement after the initial adjustment phase and before the nonlinear effects become large.

3.2.2. *Second limit: thin Debye layers and a highly conducting core*

In figure 12, the interface positions and charge q_2 at the last time step found numerically is shown for variations in the electric Weber number $\tilde{Q}$. For increasing electric effects the evolution of the interfaces slows down as indicated by a decreasing growth rate from linear theory. For larger values of $\tilde{Q}$, shown in figure 12, a satellite forms in the core fluid with an increasing size as $\tilde{Q}$ increases. This result is similar to the first limit but here the satellite is longer. In contrast to previous work on electrified

https://doi.org/10.1017/jfm.2012.145 Published online by Cambridge University Press

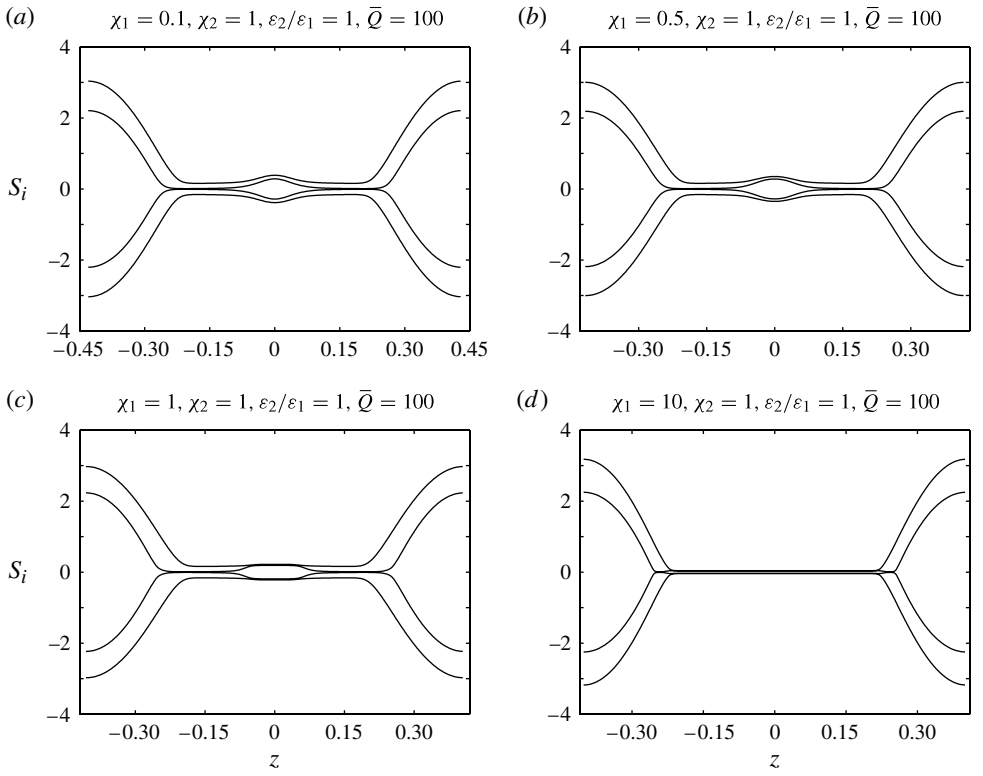


FIGURE 8. Interface radii S_1 and S_2 as a function of χ_1 for the formulation of the first limit. Here $M = 1$, $\gamma_2 = 1$, $\alpha = 1.5$, $\delta = 0.05$, $\phi_w = 1$, $R_3 = 10$, $\varepsilon_2/\varepsilon_3 = 80$ and the other parameter values are listed on the figure. The solutions are initiated from the most dangerous mode, which corresponds to k =7.3 (a), 7.52 (b), 7.73 (c) and 7.82 (d). The times associated with these profiles is $t = 27.42$ (a), 26.90 (b), 26.75 (c) and 25.5 (d).

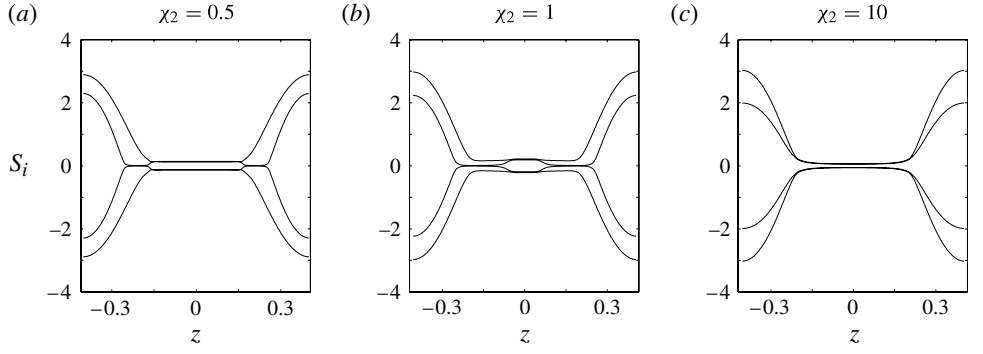


FIGURE 9. Interface radii S_1 and S_2 as a function of χ_2 for the formulation of the first limit. Here $M = 1$, $\gamma_2 = 1$, $\alpha = 1.5$, $\delta = 0.05$, $\phi_w = 1$, $R_3 = 10$ $\varepsilon_2/\varepsilon_3 = 80$, $\varepsilon_2/\varepsilon_1 = 1$, $\chi_1 = 1$, $\bar{Q} = 100$ and the other parameter values are listed in the figure. The solutions are initiated from the most dangerous mode, which corresponds to $k = 7.83$ (a), 7.73 (b) and 7.78 (c). The times associated with these profiles are $t = 27.66$ (a), 26.75 (b) and 23.5 (c).

https://doi.org/10.1017/jfm.2012.145 Published online by Cambridge University Press

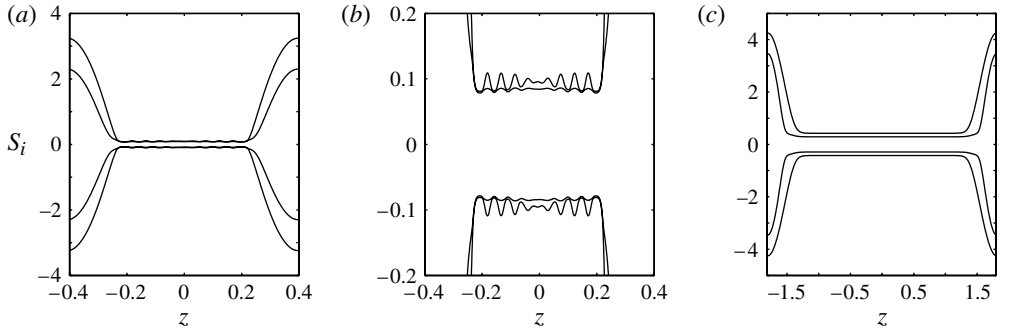


FIGURE 10. Interface radii S_1 and S_2 for $\chi_2 = 0.1$ using the formulation of the first limit. Here $M = 1$, $\gamma_2 = 1$, $\alpha = 1.5$, $\delta = 0.05$, $\phi_w = 1$, $R_3 = 10$, $\varepsilon_2/\varepsilon_3 = 80$ and $\varepsilon_2/\varepsilon_1 = 1$. The solutions are initiated from the most dangerous mode, which corresponds to $k = 7.82$ (*a*) and 1.74 (*c*). The time associated with (*a*) is $t = 52$ and the interface radii in (*c*) are stable. (*b*) Magnification of (*a*). Here (*a*) $\bar{Q} = 100$, $\chi_2 = 0.1$, (*b*) $\bar{Q} = 100$, $\chi_2 = 0.1$ and (*c*) $\bar{Q} = 400$, $\chi_2 = 0.1$.

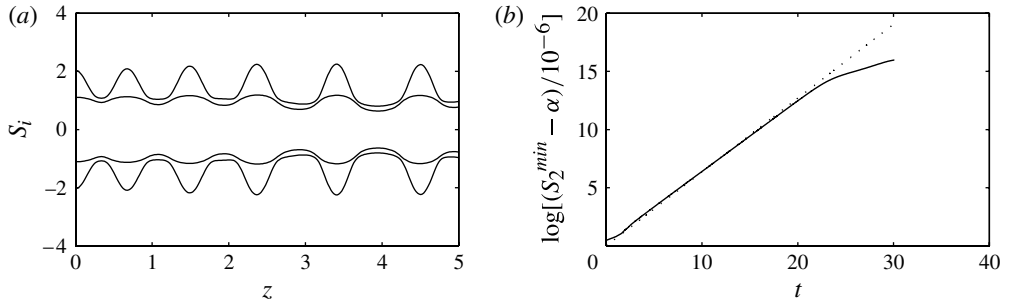


FIGURE 11. Interface position at $t = 27.5$ for the solution on a long domain ($-10 \leqslant z \leqslant 10$). The solution is initiated by uniform random disturbances applied at the outer interface with magnitude 1×10^{-6}. Panel (*b*) shows the growth rate obtained from the numerical solution (solid line) and from linear theory (dotted line). Here $\bar{Q} = 100$, $\varepsilon_2/\varepsilon_1 = 1$, $\chi_1 = \chi_2 = 1$, $M = 1$, $\gamma_2 = 1$, $\alpha = 1.5$, $\delta = 0.05$, $\phi_w = 1$, $R_3 = 10$ and $\varepsilon_2/\varepsilon_3 = 80$.

jets (Conroy *et al.* 2011*b*) in the long-wave limit, the satellite size increases with an increase in the electric Weber number, whereas for single jets the stabilizing effect of the electric field causes the satellite to be smaller. Here the electrostatic force acts on the outside of the annular fluid, slowing down its evolution and keeping the two interfaces from making contact, which allows the more viscous fluid, that evolves more slowly, to develop the satellite shape that is common in single jets.

Variations in the conductivity, $\bar{\sigma}_2$, are shown in figure 13. As noted from linear theory, increasing $\bar{\sigma}_2$ increases the growth rate and numerically causes the time to breakup to shorten. This is due to the fluids approaching that of a perfect conductor, which is more unstable than a leaky dielectric fluid at the small wavelengths studied here. The radius of the core satellite only increases slightly as $\bar{\sigma}_2$ increases and the length increases as $\bar{\sigma}_2$ decreases, partly as a result of a larger wavelength being used. For small $\bar{\sigma}_2$ the charge distribution is dominated by the transport along the gas–liquid interface by advection and we end up with profiles similar to Conroy *et al.* (2011*b*) but with peaks near the pinching location. On the other hand, for large $\bar{\sigma}_2$ the surface charge obtains a relatively large contribution from the electric field in the annular layer

https://doi.org/10.1017/jfm.2012.145 Published online by Cambridge University Press

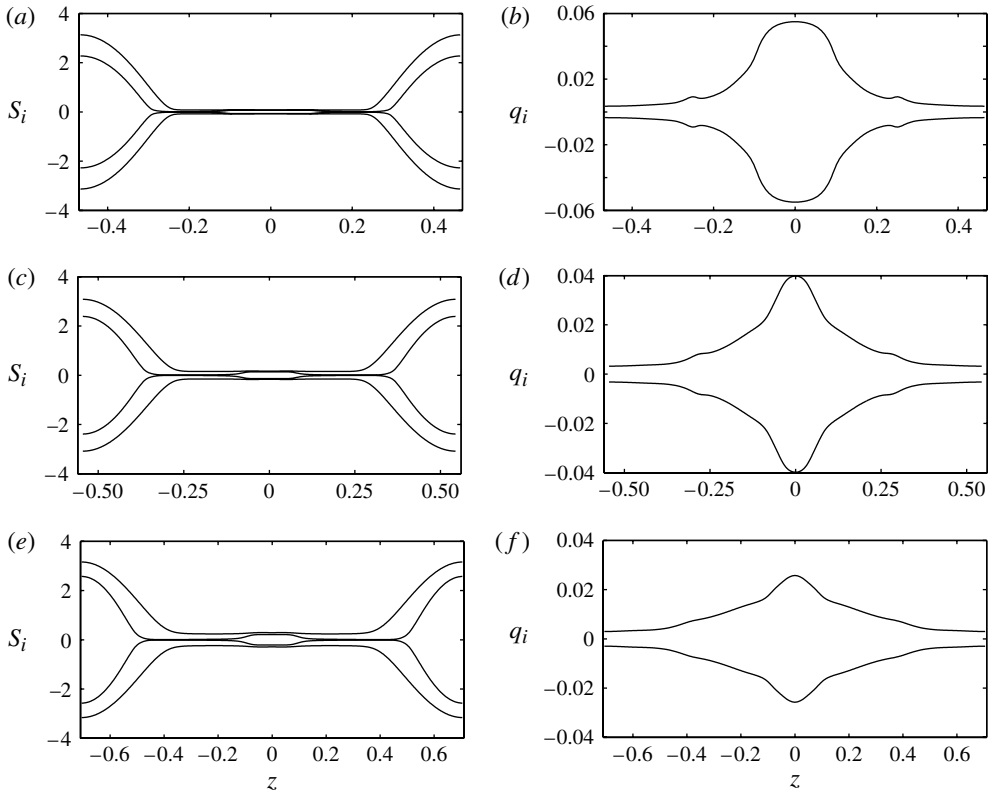


FIGURE 12. Interface radii S_1 and S_2 and charge q_2 as a function of $\tilde{Q}$ for the formulation of the second limit. Here $M = 1$, $\gamma_2 = 1$, $\alpha = 1.5$, $\delta = 0.05$, $\phi_w = 1$, $R_3 = 10$ and $\varepsilon_2/\varepsilon_3 = 80$. The solutions are initiated from the most dangerous mode, which corresponds to $k = 6.74$ (*a*), 5.76 (*c*) and 4.45 (*e*). The times associated with these profiles is $t = 31$ (*a*), 37.3 (*c*) and 43.9 (*e*). The thread is axisymmetric and we have included $\pm S$ and similarly with q_2 but note that this value is a positive quantity: (*a*) $\tilde{Q} = 300$, $\bar{\sigma}_2 = 1$, $\phi_w = 1$, $\phi_1 = 0$; (*c*) $\tilde{Q} = 400$, $\bar{\sigma}_2 = 1$, $\phi_w = 1$, $\phi_1 = 0$; and (*e*) $\tilde{Q} = 500$, $\bar{\sigma}_2 = 1$, $\phi_w = 1$, $\phi_1 = 0$.

and the surface charge has a more rounded profile. For $\bar{\sigma}_2 = 1$, shown in figure 12, the surface charge peaks at the satellite and decreases in magnitude as $\tilde{Q}$ (or $1/k$) increases.

In figure 14 the interface radii are shown as a function of the relative initial thickness of the viscous fluids, α. For small values of α, a thin outer, less viscous fluid surrounds the inner, more viscous one and a satellite does not form. From our linear stability analysis results, one expects the disturbance growth rate to increase with α (and the time to breakup to decrease, although this quantity is beyond the scope of linear theory). At $\alpha = 1.5$, a satellite forms with a drop of fluid 1 contained within a thread of fluid 2. At later times, we expect the annular fluid to break up forming a compound satellite. For $\alpha = 3$, the annular fluid drains onto the core fluid and a compound satellite forms. Variations in the relative dielectric permittivity $\varepsilon_2/\varepsilon_3$ on the final interface positions are shown in figure 15. As this ratio decreases, the growth rate of the most unstable linear mode increases, and its wavenumber decreases. For the nonlinear solutions shown in figure 15, the time to breakup and the size of the satellite increases as $\varepsilon_2/\varepsilon_3$ decreases due to the stabilizing effect of the

https://doi.org/10.1017/jfm.2012.145 Published online by Cambridge University Press

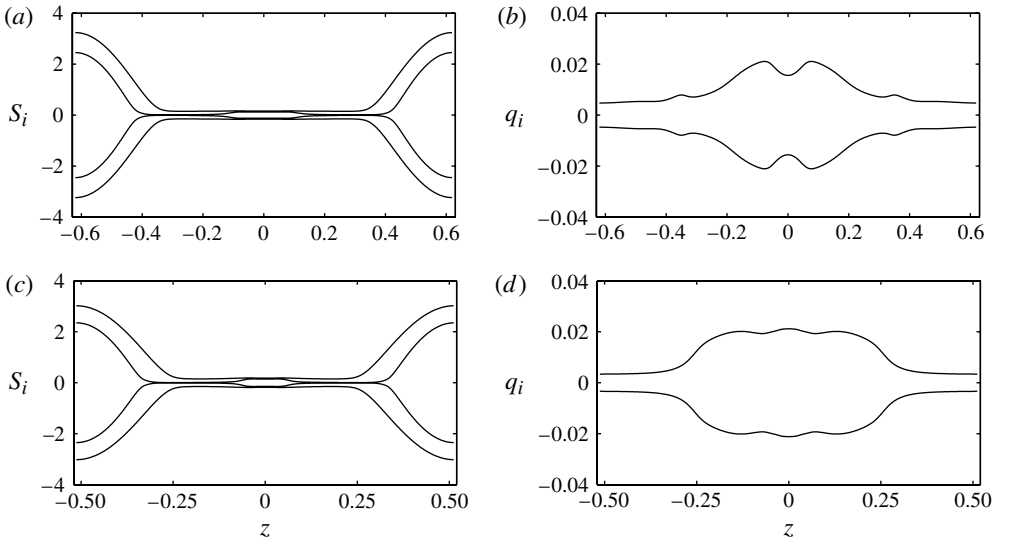


FIGURE 13. Interface radii S_1 and S_2 and charge q_2 as a function of $\bar{\sigma}_2$ for the formulation of the second limit. Here $M = 1$, $\gamma_2 = 1$, $\alpha = 1.5$, $\delta = 0.05$, $\phi_w = 1$, $R_3 = 10$ and $\varepsilon_2/\varepsilon_3 = 80$. The solutions are initiated from the most dangerous mode, which corresponds to $k = 5.065$ (*a*) and 6.125 (*c*). The times associated with these profiles is $t = 38.6$ (*a*) and 36.2 (*c*). The thread is axisymmetric and we have included $\pm S$ and similarly with q_2 but note that this value is a positive quantity: (*a*) $\tilde{Q} = 400, \bar{\sigma}_2 = 0.1, \phi_w = 1, \phi_1 = 0$; and (*c*) $\tilde{Q} = 400, \bar{\sigma}_2 = 10, \phi_w = 1, \phi_1 = 0$.

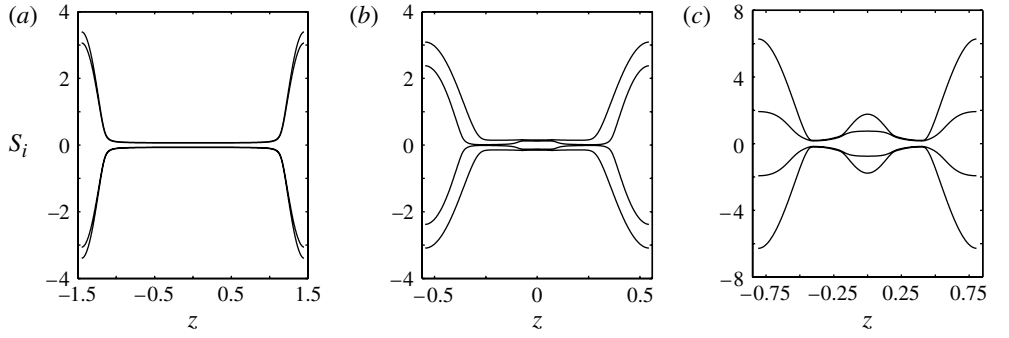


FIGURE 14. Interface radii S_1 and S_2 as a function of α for the formulation of the second limit. Here $M = 1$, $\gamma_2 = 1$, $\tilde{Q} = 400$, $\delta = 0.05$, $\phi_w = 1$, $R_3 = 10$ and $\varepsilon_2/\varepsilon_3 = 80$. The solutions are initiated from the most dangerous mode: $\lambda = 0.245$ (*a*), 0.3663 (*b*) and 2.12 (*c*), which corresponds to $k = 2.165$ (*a*), 5.76 (*b*) and 3.89 (*c*). The times associated with these profiles are $t = 45.1$ (*a*), 37.3 (*b*) and 14.5 (*c*). The thread is axisymmetric and we have included $\pm S$: (*a*) $\alpha = 1.1$; (*b*) $\alpha = 1.5$; and (*c*) $\alpha = 3$.

electric field. As discussed in the section on linear theory, the results are qualitatively similar for $\tilde{Q}$ since the permittivity ratio can be absorbed into a modified electric Weber number.

https://doi.org/10.1017/jfm.2012.145 Published online by Cambridge University Press

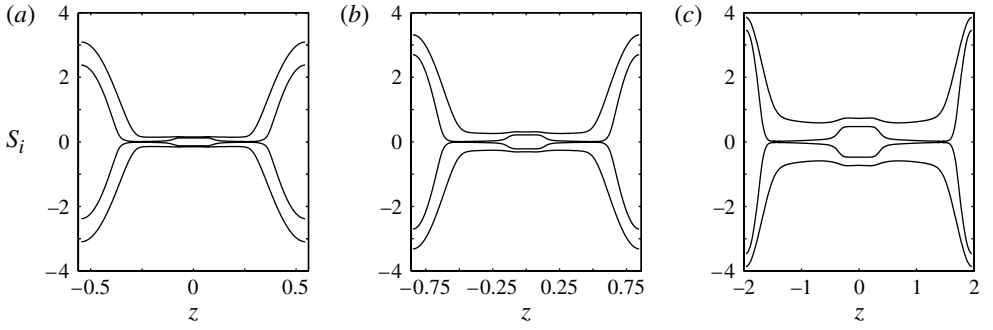


FIGURE 15. Interface radii S_1 and S_2 as a function of $\varepsilon_2/\varepsilon_3$ for the formulation of the second limit. Here $M = 1$, $\gamma_2 = 1$, $\tilde{Q} = 400$, $\delta = 0.05$, $\phi_w = 1$ and $R_3 = 10$. The solutions are initiated from the most dangerous mode: $\lambda = 0.3663$ (*a*), 0.273 (*b*) and 0.185 (*c*), which corresponds to $k = 5.76$ (*a*), 3.715 (*b*) and 1.6 (*c*). The times associated with these profiles are $t = 37.3$ (*a*), 46.25 (*b*) and 66.9 (*c*). The thread is axisymmetric and we have included $\pm S$: (*a*) $\varepsilon_2/\varepsilon_3 = 80$; (*b*) $\varepsilon_2/\varepsilon_3 = 60$; and (*c*) $\varepsilon_2/\varepsilon_3 = 40$.

4. Conclusions

In this paper we have investigated the nonlinear dynamics of an electrified, viscous compound jet using the long-wave analysis. The core fluid was assumed to be much more viscous than the annular fluid and both fluids are surrounded by a gas. The two inner fluids were taken to be electrolytes, whereas the surrounding gas is a dielectric that is in turn bounded by a radial electrode maintained at a constant voltage potential. The fluids are taken to be symmetric $z : z$ electrolytes, with the ions modelled by the Nernst–Planck equation, and providing a volumetric charge that modifies the electric field through Gauss's law. From these equations the effect of the electric field on the interfacial dynamics of compound jet breakup are investigated in two limiting cases. In the first case the surface charge at the interfaces is assumed to be small so that the electric field is continuous between the two fluids. A Maxwell's stress arises in the bulk of the fluid giving rise to electrokinetic effects. In the second case the charge is assumed to be of leading order at the interfaces and the Debye layers thin so that we recover the leaky-dielectric model.

Linear stability analysis of the one-dimensional set of equations for the two limiting cases was performed. In all cases two unstable modes were found corresponding to a stretching and squeezing mode with the latter always dominating. The electric field was found to have a stabilizing effect with both modes decreasing as the electric Weber number increased. This is attributed to the fact that the electric field creates a repulsive Debye layer and a normal electric stress at the gas–liquid interface that stabilizes the interfaces. Numerical solutions showed that the electric field slowed the drainage of the annular fluid on to the core and allowed for the formation of a satellite drop. Increasing the strength of the electric field caused the breakup time to increase and the satellite size to increase.

Acknowledgements

O.K.M. and R.V.C. would like to thank the Engineering and Physical Sciences Research Council (UK) for their support. O.K.M. would also like to acknowledge support received from the Faculty of Engineering of Imperial College to fund D.T.C. The work of D.T.P. was partly supported by NSF grant number DMS-0072228.

https://doi.org/10.1017/jfm.2012.145 Published online by Cambridge University Press

Appendix. Details of the linear theory for the second limit with thin Debye layers and a highly conducting core

Here we present the details of the linear theory for the second limit, involving the perfectly conducting core and leaky-dielectric annular fluids. We use the normal mode expansion

$$(S_1, S_2, w_1, q_2) = (1, \alpha, 0, q_{20}) + (\hat{S}_1, \hat{S}_2, \hat{w}_1, \hat{q}_2) \tag{A 1}$$

where hats denote small perturbations, α is the ratio of outer to inner undisturbed positions and the charge at the basic state is found from (2.78) at zero velocity to be

$$q_{20} = \frac{\left(\sigma_3\dfrac{\varepsilon_2}{\varepsilon_3} - \sigma_2\right)(\phi_w - \phi_1)}{\left(\sigma_3\dfrac{\varepsilon_2}{\varepsilon_3}\right)\left(\alpha\ln(\alpha) - \alpha\dfrac{\varepsilon_2}{\varepsilon_3}\ln(\alpha/R_3)\right) + \left(\sigma_3\dfrac{\varepsilon_2}{\varepsilon_3} - \sigma_2\dfrac{\varepsilon_2}{\varepsilon_3}\right)\alpha\ln(\alpha/R_3)} \tag{A 2}$$

and define the following $f_1 = \phi_{20r}|_{S_1}$, $f_2 = \phi_{20r}|_{S_2}$, $f_3 = \phi_{30r}|_{S_2}$, $f_4 = \phi_2|_{S_2}$, $f_5 = f_1^2$, $f_6 = f_2^2$ and $f_7 = f_3^2$. Using (A 1), linearization of the kinematic conditions, surface charge and axial velocity at interface 1 yields the following

$$\hat{S}_{1t} = -\frac{1}{2}\hat{w}_{1z}, \tag{A 3}$$

$$\hat{S}_{2t} = \hat{u}_2|_{\alpha, q_{20}}, \tag{A 4}$$

$$\hat{q}_{2t} + q_{20}\left(\hat{w}_{2z} + \alpha^{-1}\hat{u}_2\right) \tag{A 5}$$

$$= \hat{S}_1\left(\bar{\sigma}_3\frac{\partial f_3}{\partial S_1} - \bar{\sigma}_2\frac{\partial f_2}{\partial S_1}\right) + \hat{S}_2\left(\bar{\sigma}_3\frac{\partial f_3}{\partial S_2} - \bar{\sigma}_2\frac{\partial f_2}{\partial S_2}\right) + \hat{q}_2\left(\bar{\sigma}_3\frac{\partial f_3}{\partial q_2} - \bar{\sigma}_2\frac{\partial f_2}{\partial q_2}\right) \tag{A 6}$$

$$\bar{Re}\hat{w}_{1t} - 3\hat{w}_{1zz} - (\hat{S}_{1z} + \delta^2\hat{S}_{1zzz}) - \gamma_2(\hat{S}_{2z} + \alpha^2\delta^2\hat{S}_{2zzz}) = C_1\hat{S}_{1z} + C_2\hat{S}_{2z} + C_3\hat{q}_{2z} \tag{A 7}$$

where the radial and axial velocity at S_2 and constant $\hat{K}_{2zz}$ are defined as

$$\hat{u}_2|_\alpha = -\frac{\alpha}{2}\hat{w}_{1z} + D_6\hat{K}_{2zz} + D_7\hat{f}_{4zz}, \tag{A 8}$$

$$\hat{w}_{2z} = D_5\hat{K}_{2zz} + \hat{w}_{1z} - D_4\ln(\alpha)\hat{f}_{4zz} \tag{A 9}$$

$$\hat{K}_{2zz} = \frac{-\gamma_2}{\alpha^2}(\hat{S}_{2zz} + \delta^2\alpha^2\hat{S}_{2zzzz}) + \frac{\tilde{Q}}{2}(D_1\hat{S}_{1zz} + D_2\hat{S}_{2zz} + D_3\hat{q}_{2zz}). \tag{A 10}$$

The constants appearing above are

$$D_1 = \frac{\partial f_6}{\partial S_1} - \frac{\varepsilon_2}{\varepsilon_3}\frac{\partial f_7}{\partial S_1}, \quad D_2 = \frac{\partial f_6}{\partial S_2} - \frac{\varepsilon_2}{\varepsilon_3}\frac{\partial f_7}{\partial S_2}, \quad D_3 = \frac{\partial f_6}{\partial q_2} - \frac{\varepsilon_2}{\varepsilon_3}\frac{\partial f_7}{\partial q_2}, \tag{A 11}$$

$$D_4 = \frac{2\xi\tilde{Q}\alpha q_{20}}{M}, \quad D_5 = \frac{1}{4M}(\alpha^2 - 2\alpha^2\ln(\alpha) - 1), \tag{A 12}$$

$$D_6 = \frac{1}{4M}\left(-\frac{3\alpha^3}{4} + \alpha - \frac{\alpha^{-1}}{4} + \alpha^3\ln(\alpha)\right), \quad D_7 = \frac{D_4}{4\alpha} + \frac{D_4\alpha}{2}\left(\ln(\alpha) - \frac{1}{2}\right), \tag{A 13}$$

https://doi.org/10.1017/jfm.2012.145 Published online by Cambridge University Press

$$D_8 = q_{20}D_5 + \frac{q_{20}D_6}{4M\alpha}, \quad D_9 = \frac{q_{20}D_7}{\alpha} - q_{20}D_4\ln(\alpha), \tag{A 14}$$

$$C_1 = \frac{\tilde{Q}}{2}\frac{\partial f_5}{\partial S_1} - \frac{\tilde{Q}}{2}\alpha^2 D_1 - \frac{2D_4}{M}\frac{\partial f_4}{\partial S_1}, \tag{A 15}$$

$$C_2 = \frac{\tilde{Q}}{2}\frac{\partial f_5}{\partial S_2} - \frac{\tilde{Q}}{2}\alpha^2 D_2 - \frac{2D_4}{M}\frac{\partial f_4}{\partial S_2}, \tag{A 16}$$

$$C_3 = \frac{\tilde{Q}}{2}\frac{\partial f_5}{\partial q_2} - \frac{\tilde{Q}}{2}\alpha^2 D_3 - \frac{2D_4}{M}\frac{\partial f_4}{\partial q_2}. \tag{A 17}$$

Substitution of the normal mode expansion

$$(\hat{S}_1, \hat{S}_2, \hat{w}_1, \hat{q}_2) = (\bar{S}_1, \bar{S}_2, \bar{w}_1, \bar{q}_2)\mathrm{e}^{\lambda t + \mathrm{i}kz} \tag{A 18}$$

yields the linear system of equations

$$\lambda\bar{S}_1 + \frac{\mathrm{i}k}{2}\bar{w}_1 = 0 \tag{A 19}$$

$$\lambda\bar{S}_2 + N_1\bar{S}_1 + N_2\bar{S}_2 + \frac{\mathrm{i}k\alpha}{2}\bar{w}_1 + N_3\bar{q}_2 = 0 \tag{A 20}$$

$$\lambda\bar{w}_1 + \frac{N_5\mathrm{i}k}{\bar{R}_e}\bar{S}_1 + \frac{N_6\mathrm{i}k}{\bar{R}_e}\bar{S}_2 + \frac{N_4}{\bar{R}_e}\bar{w}_1 + \frac{N_7\mathrm{i}k}{\bar{R}_e}\bar{q}_2 = 0 \tag{A 21}$$

$$\lambda\bar{q}_2 + N_9\bar{S}_1 + N_{10}\bar{S}_2 + \mathrm{i}kN_{11}\bar{w}_1 + \bar{q}_2N_8 = 0 \tag{A 22}$$

where the constants are given as

$$N_1 = \frac{D_6\tilde{Q}k^2D_1}{8M} + k^2D_7\frac{\partial f_4}{\partial S_1} \tag{A 23}$$

$$N_2 = \frac{D_6}{4M}\frac{\gamma_2}{\alpha^2}(-k^2 + \delta^2\alpha^2k^4) + \frac{D_6\tilde{Q}k^2D_2}{8M} + k^2D_7\frac{\partial f_4}{\partial S_2} \tag{A 24}$$

$$N_3 = \frac{D_6\tilde{Q}k^2D_3}{8M} + k^2D_7\frac{\partial f_4}{\partial q_2} \tag{A 25}$$

$$N_4 = 3k^2 \tag{A 26}$$

$$N_5 = -C_1 - 1 + k^2\delta^2 \tag{A 27}$$

$$N_6 = -C_2 - \gamma_2 + \gamma_2k^2\delta^2\alpha^2 \tag{A 28}$$

$$N_7 = -C_3 \tag{A 29}$$

$$N_8 = -\frac{D_8D_3\tilde{Q}k^2}{2} - D_9k^2\frac{\partial f_4}{\partial q_2} - \bar{\sigma}_3\frac{\partial f_3}{\partial q_2} + \bar{\sigma}_2\frac{\partial f_2}{\partial q_2} \tag{A 30}$$

$$N_9 = -\frac{D_8D_1\tilde{Q}k^2}{2} - D_9k^2\frac{\partial f_4}{\partial S_1} - \bar{\sigma}_3\frac{\partial f_3}{\partial S_1} + \bar{\sigma}_2\frac{\partial f_2}{\partial S_1} \tag{A 31}$$

$$N_{10} = D_8\frac{\gamma_2}{\alpha^2}(k^2 - \delta^2\alpha^2k^4) - \frac{\tilde{Q}}{2}D_8D_2k^2 - D_9k^2\frac{\partial f_4}{\partial S_2} - \bar{\sigma}_3\frac{\partial f_3}{\partial S_2} + \bar{\sigma}_2\frac{\partial f_2}{\partial S_2} \tag{A 32}$$

$$N_{11} = q_{20}/2. \tag{A 33}$$

https://doi.org/10.1017/jfm.2012.145 Published online by Cambridge University Press

REFERENCES

BORWANKAR, R. P. & WASAN, D. T. 1986 The kinetics of adsorption of ionic surfactants at gas–liquid interfaces. *Chem. Engng Sci.* **41**, 199–201.

BORWANKAR, R. P. & WASAN, D. T. 1988 Equilibrium and dynamics of adsorption of surfactants at fluid–fluid interfaces. *Chem. Engng Sci.* **219**, 1323–1337.

CHANG, H.-C. & FRANSES, E. I. 1995 Adsorption dynamics of surfactants at the air/water interface: a critical review of mathematical models, data, and mechanisms. *Colloids Surf.* **100**, 1–45.

CHANG, H.-C. & YEO, L. Y. 2010 *Electrokinetically Driven Microfluidics and Nanofluidics*. Cambridge University Press.

CHAUHAN, A., MALDARELLI, C., PAPAGEORGIOU, D. T. & RUMSCHITZKI, D. S. 2000 Temporal instability of compound threads and jets. *J. Fluid Mech.* **420**, 1–25.

CHAUHAN, A., MALDARELLI, C., RUMSCHITZKI, D. S. & PAPAGEORGIOU, D. T. 1996 Temporal and spatial instability of an inviscid compound jet. *Rheol. Acta* **35**, 567–583.

CHEN, X., JIA, L., YIN, X. & CHENG, J. 2005 Spraying modes in coaxial jet electrospray with outer driving liquid. *Phys. Fluids* **17**, 1–7.

COLLINS, R. T., HARRIS, M. T. & BASARAN, O. A. 2007 Breakup of electrified jets. *J. Fluid Mech.* **588**, 75–129.

CONROY, D. T., CRASTER, R. V., MATAR, O. K. & PAPAGEORGIOU, D. T. 2010 Dynamics and stability of an annular electrolyte film. *J. Fluid Mech.* **656**, 481–506.

CONROY, D. T., MATAR, O. K., CRASTER, R. V. & PAPAGEORGIOU, D. T. 2011*a* Breakup of an electrified, perfectly conducting, viscous thread in an ac field. *Phys. Rev.* E **83**.

CONROY, D. T., MATAR, O. K., CRASTER, R. V. & PAPAGEORGIOU, D. T. 2011*b* Breakup of an electrified viscous thread with charged surfactants. *Phys. Fluids* **23**, 1–19.

CRASTER, R. V., MATAR, O. K. & PAPAGEORGIOU, D. T. 2003 Pinchoff and satellite formation in compound viscous threads. *Phys. Fluids* **15**, 3409–3428.

CRASTER, R. V., MATAR, O. K. & PAPAGEORGIOU, D. T. 2005 On compound liquid threads with large viscosity contrasts. *J. Fluid Mech.* **533**, 95–124.

DAVIES, J. T. & RIDEAL, E. K. 1961 *Interfacial Phenomena*. Academic.

DENN, M. M. 1980 Continuous drawing of liquids to form fibres. *Annu. Rev. Fluid Mech.* **12**, 365–387.

HAMMOND, P. S. 1983 Nonlinear adjustment of a thin annular film of viscous fluid surrounding a thread of another within a circular cylindrical pipe. *J. Fluid Mech.* **137**, 363–384.

HARDAS, N., DANVIRIYAKUL, S., FOLEY, J. L., NAWAR, W. W. & CHINACHOTI, P. 2000 Accelerated stability studies of microencapsulated anhydrous milk fat. *Lebensmittel-Wiss. Technol. (Food Sci. Technol.)* **33**, 506–513.

HERTZ, C. H. & HERMANRUD, B. 1983 A liquid compound jet. *J. Fluid Mech.* **131**, 271.

HIGUERA, F. J. 2007 Stationary coaxial electrified jet of a dielectric liquid surrounded by a conductive liquid. *Phys. Fluids* **19**, 1–9.

HUEBNER, A. L. & CHU, H. N. 1971 Instability and breakup of charged liquid jets. *J. Fluid Mech.* **49**, 361–372.

KALLIADASIS, S. & CHANG, H.-C. 1994 Drop formation during the coating of vertical fibres. *J. Fluid Mech.* **261**, 135–168.

LEE, Y. H., KIM, C. A., JANG, W. H., CHOI, H. J. & JHON, M. S. 2001 Synthesis and electrorhelogical characteristics of microencapsulated polyaniline particles with melamine-formaldehyde resins. *Polymer* **42**, 8277–8283.

LI, F., YIN, X. Y. & YIN, X. Z. 2005 Linear instability analysis of an electrified coaxial jet. *Phys. Fluids* **17**, 1–12.

LI, F., YIN, X. Y. & YIN, X. Z. 2006 Instability analysis of a coaxial jet under a radial electric field in the nonequipotential case. *Phys. Fluids* **18**, 1–13.

LI, F., YIN, X. Y. & YIN, X. Z. 2008 Instability of a viscous coflowing jet in a radial electric field. *J. Fluid Mech.* **596**, 285–311.

LOSCERTALES, I. G., BARRERO, A., GUERRERO, I., CORTIJO, R., MARQUEZ, M. & GANAN-CALCO, A. M. 2002 Micro/nano encapsulation via electrifed coaxial liquid jets. *Science* **295**, 1695–1698.

https://doi.org/10.1017/jfm.2012.145 Published online by Cambridge University Press

PAPAGEORGIOU, D. T. 1995 On the breakup of viscous liquid threads. *Phys. Fluids* **7**, 1529–1544.

PROSSER, A. J. & FRANCES, E. I. 2001 Adsorption and surface tension of ionic surfactants at the air–water interface: review and evaluation of equilibrium models. *Colloids Surf.* A **178**, 1–40.

RADEV, S. & SHKADOV, V. 1985 On the stability of two-layer capillary jet. *Theor. Appl. Mech.* **16**, 68.

RADEV, S. & TCHAVDAROV, B. 1988 Linear capillary instability of compound jets. *Intl J. Multiphase Flow* **14**, 67–79.

SANZ, A. & MESEGUER, J. 1985 One-dimensional analysis of the compound jet. *J. Fluid Mech.* **159**, 55–68.

SAVILLE, D. A. 1997 Electrohydrodynamics: the Taylor–Melcher leaky-dielectric model. *Annu. Rev. Fluid Mech.* **29**, 27.

SURYO, R., DOSHI, P. & BASARAN, O. A. 2006 Nonlinear dynamics and breakup of compound jets. *Phys. Fluids* **18**, 1–31.

WANG, Q., MAHLMANN, S. & PAPAGEORGIOU, D. T. 2009 Dynamics of liquid jets and threads under the action of radial electric fields: Microthread formation and touchdown singularities. *Phys. Fluids* **21**, 1–19.

WILKES, E. D., PHILLIPS, S. D. & BASARAN, O. A. 1999 Computational and experimental analysis of dynamics of drop formation. *Phys. Fluids* **11**, 3577–3598.

https://doi.org/10.1017/jfm.2012.145 Published online by Cambridge University Press